NAVAL POSTGRADUATE SCHOOL

MONTEREY, CALIFORNIA

THESIS

FEASIBILITY STUDY TO ADAPT THE MICROFLOWN VECTOR SENSOR FOR UNDERWATER USE

by

Marnix J.M. Hezemans

December 2012

Thesis Advisor:	Kevin B. Smith
Second Reader:	Daphne Kapolka

Approved for public release; distribution is unlimited

THIS PAGE INTENTIONALLY LEFT BLANK

REPORT DOCUMENTATION PAGE			Form Approved OMB No. 0704–0188
Public reporting burden for this collection of information is estimated to average 1 hour per response, including the time for reviewing instruction, searching existing data sources, gathering and maintaining the data needed, and completing and reviewing the collection of information. Send comments regarding this burden estimate or any other aspect of this collection of information, including suggestions for reducing this burden, to Washington headquarters Services, Directorate for Information Operations and Reports, 1215 Jefferson Davis Highway, Suite 1204, Arlington, VA 22202–4302, and to the Office of Management and Budget, Paperwork Reduction Project (0704–0188) Washington DC 20503.			
1. AGENCY USE ONLY *(Leave blank)*	**2. REPORT DATE** December 2012	**3. REPORT TYPE AND DATES COVERED** Master's Thesis	
4. TITLE AND SUBTITLE FEASIBILITY STUDY TO ADAPT THE MICROFLOWN VECTOR SENSOR FOR UNDERWATER USE		**5. FUNDING NUMBERS**	
6. AUTHOR(S) Marnix J.M. Hezemans			
7. PERFORMING ORGANIZATION NAME(S) AND ADDRESS(ES) Naval Postgraduate School Monterey, CA 93943–5000		**8. PERFORMING ORGANIZATION REPORT NUMBER**	
9. SPONSORING /MONITORING AGENCY NAME(S) AND ADDRESS(ES) N/A		**10. SPONSORING/MONITORING AGENCY REPORT NUMBER**	
11. SUPPLEMENTARY NOTES The views expressed in this thesis are those of the author and do not reflect the official policy or position of the Department of Defense or the U.S. Government. IRB Protocol number ____N/A____.			
12a. DISTRIBUTION / AVAILABILITY STATEMENT Approved for public release; distribution is unlimited		**12b. DISTRIBUTION CODE**	

13. ABSTRACT (maximum 200 words)

This thesis investigates the feasibility of adapting the Microflown PU match vector sensor for underwater use. After testing the proper functioning of the sensor, the best materials for the capsule are determined based on acoustic properties. The capsule is designed and built by NPS staff. To predict the sensitivity of the encapsulated sensor, the characteristic equations are modified to reflect the new medium. In order to be able to predict the sensitivity of the encapsulated sensor, the performance ratio is determined between the sensitivity in air and the filling fluid of choice. Temperature dependency is introduced in the relevant parameters to be able to model the sensitivity at various operating temperatures. The measured sensitivity from the calibration report is then used to predict its performance in castor oil. The theoretical sensitivity model is verified by experimental data gathered from calibration studies at NUWC. The verified model is then used to analyze the consequences of changing critical operating parameters like the distance between the filaments and the operating temperature. Based on these calculations, recommendations are made for a better performing prototype. Eventually a new design is proposed that increases sensitivity significantly and is better adapted to operate in the filling fluid.

14. SUBJECT TERMS Microflown, underwater sound detection, vector sensor, temperature dependency			**15. NUMBER OF PAGES** 91
			16. PRICE CODE
17. SECURITY CLASSIFICATION OF REPORT Unclassified	**18. SECURITY CLASSIFICATION OF THIS PAGE** Unclassified	**19. SECURITY CLASSIFICATION OF ABSTRACT** Unclassified	**20. LIMITATION OF ABSTRACT** UU

NSN 7540–01–280–5500

Standard Form 298 (Rev. 2–89)
Prescribed by ANSI Std. 239–18

THIS PAGE INTENTIONALLY LEFT BLANK

Approved for public release; distribution is unlimited

FEASIBILITY STUDY TO ADAPT THE MICROFLOWN VECTOR SENSOR FOR UNDERWATER USE

Marnix J.M. Hezemans, Lieutenant Commander, Royal Netherlands Navy

Submitted in partial fulfillment of the
requirements for the degree of

MASTER OF SCIENCE IN ENGINEERING ACOUSTICS

from the

NAVAL POSTGRADUATE SCHOOL
December 2012

Author: Marnix J.M. Hezemans

Approved by: Kevin B. Smith
Thesis Advisor

Daphne Kapolka
Second Reader

Daphne Kapolka
Chair, Engineering Acoustics Academic Committee

THIS PAGE INTENTIONALLY LEFT BLANK

ABSTRACT

This thesis investigates the feasibility of adapting the Microflown PU match vector sensor for underwater use. After testing the proper functioning of the sensor, the best materials for the capsule are determined based on acoustic properties. The capsule is designed and built by NPS staff. To predict the sensitivity of the encapsulated sensor, the characteristic equations are modified to reflect the new medium. In order to be able to predict the sensitivity of the encapsulated sensor, the performance ratio is determined between the sensitivity in air and in the filling fluid of choice. Temperature dependency is introduced in the relevant parameters to be able to model the sensitivity at various operating temperatures. The measured sensitivity from the calibration report is then used to predict its performance in castor oil. The theoretical sensitivity model is verified by experimental data gathered from calibration studies at NUWC. The verified model is then used to analyze the consequences of changing critical operating parameters like the distance between the filaments and the operating temperature. Based on these calculations, recommendations are made for a better performing prototype. Eventually a new design is proposed that increases sensitivity significantly and is better adapted to operate in the filling fluid.

THIS PAGE INTENTIONALLY LEFT BLANK

TABLE OF CONTENTS

LIST OF FIGURES

THIS PAGE INTENTIONALLY LEFT BLANK

LIST OF TABLES

THIS PAGE INTENTIONALLY LEFT BLANK

LIST OF ACRONYMS AND ABBREVIATIONS

IL	Intensity Level
NSL	Noise Spectrum Level
NUWC	Naval Undersea Warfare Centre
NPS	Naval Postgraduate School
SN	Self Noise
SPL	Sound Pressure Level
F_s	Sampling frequency
NI cDAQ	National Instruments compact Data Acquisition box

THIS PAGE INTENTIONALLY LEFT BLANK

ACKNOWLEDGMENTS

I wish to thank my wonderful wife, Sanne, for agreeing to go on this adventure with me. I know that postponing your job as a midwife in the Netherlands and being abroad in this troubled time of our families was sometimes very hard for you. Without your unwavering support to me and our family, I would never have been able to get this degree. To my kids, Thije and Lieve, I am so happy that after long days I could come home to your unconditional love, laughter and energy. I will thoroughly enjoy all our new adventures upon returning to Holland.

I would like to thank my thesis advisor, Kevin Smith, for his hands-off approach in completing this thesis. It allowed me to really tackle the problem at hand in my own way, but with the knowledge that I could always come to you for guidance when I was stuck.

Furthermore, I would like to thank Daphne Kapolka for teaching me, among many things, the power of averaging. I appreciate your critical and inquisitive nature as well as your great hospitality.

Then, I would like to thank Jay Adeff for not killing me after I ruined his experimental setup and, of course, for his design and construction of the capsule for the Microflown.

I would like to thank NPS faculty and staff for creating such a comfortable but still very challenging learning environment.

Finally, I would like to thank all my fellow students in the applied physics, engineering acoustics and undersea warfare track for their friendship. You made this M.S. degree a generally enjoyable experience. I hope to be able to visit some of you in the future!

THIS PAGE INTENTIONALLY LEFT BLANK

I. INTRODUCTION

A. THE PRINCIPLE OF HOT WIRE ANEMOMETRY

Hot wire anemometers have been used in fluid mechanics since the late 1800s. These thermal transducers are widely used to study turbulence and unsteady laminar flows. The principle of hot wire anemometry is relatively simple. A current is passed through a fine filament. When molecules flow by the filament they will transfer heat away from the wire. The rate of heat transfer will be determined by the flow speed and flow temperature, as well as the physical properties of the medium and filament. The cooling of the wire will change the resistance of the filament. The variation in the resistance can be measured.

There are two basic modes of operation. The most common is the constant current mode, where the current though the filament is kept constant. The voltage difference to accomplish this will vary with the change in resistance of the filament. The voltage difference thus becomes a measure for the flow speed and temperature. A different mode of operation is the constant temperature mode. This mode will keep the filament at a constant temperature. In order to do this a feedback circuit will hold the resistance of the wire constant by varying the current through the wire to compensate for the heat transfer by the flow. The current thus becomes a measure for the flow speed and temperature.

The advantage of measuring a flow by using a hot filament is the large bandwidth. A hot wire can measure flow speed easily from DC-flows to over 400 kHz. Furthermore a hot wire anemometer has very good sensitivity as well as spatial resolution.

However, a hot wire anemometer is very easily damaged due to the exposed thin wires. Additionally, a hot wire anemometer is a non-linear system. This will complicate its calibration process [1]. Finally, a hot wire anemometer needs a minimum flow speed of about 1 cm/s to function properly.

B. THE MICROFLOWN PU MATCH

The Dutch company Microflown Technologies has taken a different approach in order to be able to measure lower particle velocities using hot filaments, using two parallel filaments in close proximity. The temperature upstream is slightly less than the temperature downstream. Therefore, the downstream wire is heated more by the upstream wire and vice versa when the flow changes direction. The temperature difference between the two wires then becomes a measure for the flow speed and direction. Using this principle it can operate in a flow range of 100 nm/s to 1 m/s [2]. In air, this means that sound pressure levels (SPL) from $3.3dB$ to $143dB$ re $20\mu Pa$ can be measured. These dB values represent sound just over the sensitivity threshold of the human ear to well over the pain threshold. In seawater particle velocities are much smaller due to the increased impedance of the medium.

The Microflown Technologies "PU match" sensor adds a miniature pressure microphone (P) to a single axis Microflown velocity (U) sensor to form a package the size of a match. The velocity sensor measures the magnitude of the acoustic particle velocity along its axis. Combining the signal from the velocity sensor with a pressure microphone enables the sensor to resolve whether the source is in the positive or the negative direction along the axis and to determine the intensity of sound transmitted along the axis across a wide bandwidth (20 Hz–20 kHz).

C. POTENTIAL FOR UNDERWATER SOUND DETECTION

Although many properties are the same for both the hot wire anemometer and the Microflown PU match, there are two properties that motivate us only to consider the Microflown PU match. In water, the particle displacement and velocity are much smaller than in air, but the particle density is much higher. Since the Microflown PU match can measure much smaller flow speeds, it is much better suited for underwater sound detection than traditional hot wire anemometers. In addition, its beam pattern is a figure eight, which makes unambiguous directionality possible by adding a pressure microphone.

There are several reasons why it is interesting to examine the possibility to adapt the Microflown PU match for underwater sound detection. In the first place, it would be able to determine direction of sound without the need for long arrays. This is similar to the advantage of traditional underwater vector sensors based on accelerometer technology. Second, the response covers a very large bandwidth with a single sensor. Moreover the Microflown PU match has very good sensitivity at very low frequencies. Since the attenuation of low frequency sound in the ocean is much less than that of high frequencies, this capability could improve detection ranges. And finally, the small size of the sensor would enable integration in the sensor suite of very small systems.

D. ENCAPSULATION OF THE MICROFLOWN PU MATCH

The corrosive properties of seawater make encapsulation of the sensor necessary. This provides challenges common to underwater sound transducers. The encapsulation should be some kind of outer shell filled with a non-conducting liquid (usually oil based). In order to reduce reflection losses the impedance of both the shell and the liquid must be matched to the impedance of seawater. This impedance match will also limit refraction, which will introduce uncertainty in the source direction.

It is therefore important to carefully determine the materials used for the encapsulation. Since resources were limited, the choice of outer shell materials was primarily based on the molding properties and less on acoustics. The choice of filling fluid was however carefully based on acoustical properties.

This research is conducted to determine the feasibility to use this sensor for underwater sound detection. At this point, there is no requirement for operational flexibility. No effort will be put into enabling the sensor to operate in a wide depth and/or temperature range.

The encapsulation approach was designed and executed by Jay Adeff (NPS staff) and the details will not be a part of this thesis. A general description will be provided.

E. STRUCTURE OF THIS THESIS

In this thesis, the performance of the sensor in air at room temperature will first be evaluated. This will allow us to determine if the sensor is working properly and compare the performance underwater with its performance in air, for which it was designed. The sensor performance underwater will then be predicted. The calibration tests to evaluate the performance of the sensor underwater will be executed at the Naval Undersea Warfare Center (NUWC) Division Newport's Undersea Sound Reference Division and, due to facilities access, by NUWC staff. Data from the experiments will then be compared to the predictions and its performance will be evaluated. The degree to which alterations of the current sensor will influence its performance underwater will then be examined. Finally, conclusions will be drawn and recommendations will be made for the way ahead.

II. EVALUATION OF THE MICROFLOWN PU MATCH IN AIR

A. INTRODUCTION

The Microflown PU match is a one-dimensional acoustic vector sensor. It consists of a conventional miniature Knowles FG-series pressure sensor and a Microflown Titan acoustical velocity sensor element. The sensor, as shown in Figure 1, is designed to operate in air between 20 Hz–20 kHz. The sensor is 45 mm long and has a width of 3.5 mm, roughly the size of a matchstick. The upper sensor element is the conventional pressure microphone. The lower sensor is the Microflown Titan sensor element. In the sensor used for this thesis, the Titan sensor element was oriented across the stem of the pressure microphone element, resulting in a particle velocity axis at right angles to the stem.

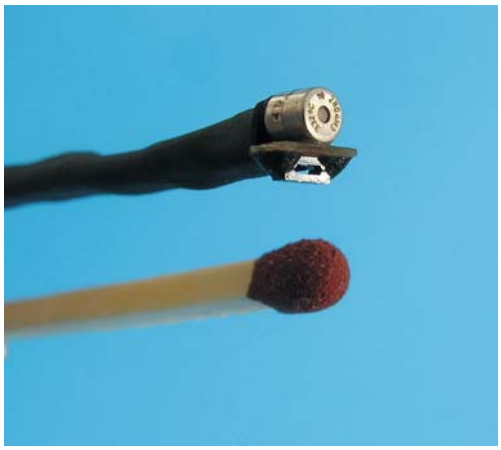

Figure 1. Microflown PU match (picture by Microflown Technologies)

To verify its proper functioning and to be able to compare underwater performance to performance in the medium for which it was designed, the sensor was first evaluated in air. The primary goal was to establish the transfer function of the sensor and to see if the pressure and acoustical velocity sensors were coherent. The secondary goal was to compare the performance of the Microflown PU match sub-sensors to a well-

known pressure sensor; the ACO Pacific model 7046. The beam pattern of the Microflown Titan sensor was also determined. These measurements were all conducted in the anechoic chamber at NPS.

B. THE TRANSFER FUNCTION

1. Method

The method used to establish the transfer function in air was based on previous work by Chee Wee Ng and Jeffrey Caulk [3], [4]. To determine the transfer function, the sensor was placed in front of an Austin AU-15G sound source. See Appendix A for a comprehensive list of all equipment used in the measurements. The sound source, a guitar amplifier, was chosen primarily for its ability to produce loud noise over a bandwidth of 100 Hz–2 kHz. Other acoustical properties were of less importance for this experiment. A calibrated ACO Pacific pressure microphone in combination with an ACO pacific 1/2" preamplifier was installed above the Microflown at a distance of 3.2 cm. An HP 33120A Arbitrary Waveform Generator was used to produce white noise with amplitude of $10V_{pp}$. The far field condition, providing the range at which wave front curvature may be neglected, for a frequency of 2 kHz at 20° Celsius [5] is

$$FF = \frac{\pi R^2}{\lambda} = \frac{\pi(0.032m)^2}{0.17m} = 0.02m \tag{1}$$

The distance between source and sensor was 2.04 meter and therefore well in the far field.

Data acquisition during this experiment was conducted using the Mathworks Matlab data acquisition toolbox that enabled direct data import from the National Instruments cDAQ (NI cDAQ). In the system configuration used, the NI cDAQ had a maximum sampling rate of 51.2 kHz. The sampling rates that could be selected can be determined by the following formula [6]:

$$f_s = \frac{f_m / 256}{n}, \tag{2}$$

where f_s is the sampling frequency, f_m represents the master clock rate (13.1072 MHz) and n an integer between 1 and 31. Since the bandwidth of interest for this thesis is 20 Hz–2.0 kHz, a chosen sampling frequency of 4267 Hz is just above the Nyquist frequency. This corresponds with $n = 12$.

2. The Result

The estimate of the transfer function started by establishing the frequency range over which the two sensor elements were coherent. This was done using the Matlab command `mscohere`. The coherence between pressure and velocity sensor elements increased significantly with higher source levels. The actual transfer function estimate between the pressure element (p) and the velocity sensor (v) was calculated by

$$\left\langle \hat{H}_v(k) \right\rangle = \frac{\left\langle \hat{X}_p(k)\hat{X}_v^*(k) \right\rangle}{\left\langle \hat{X}_v(k)\hat{X}_v^*(k) \right\rangle}, \tag{3}$$

where $\hat{H}_v(k)$ is the transfer function of the k^{th} frequency bin and $\hat{X}_v(k)$ is the digital Fourier transform (DFT) of the time-domain signals. For better precision three datasets were used to compute an average transfer function. Figure 2 shows the average transfer function for the Microflown PU match and the coherence between the pressure element and the particle velocity element. The full analysis and computer code can be found in Appendix B. The output is coherent in the bandwidth 80 Hz–2.0 kHz. Increasing the source level had a significant effect on the coherence. Technical limitations of the equipment used prevented further exploration of the low end coherence. The transfer function established during the measurements is not smooth. This may be the result of reflections from the test setup or some airflow in the room. The amplitude of the transfer function from the pressure sensor element to the velocity sensor element shows the same trend as follows from the calibration report. The phase difference plot also follows the prediction from the calibration report. From this it can be concluded that the Microflown PU match is measuring particle vibrations and performs as stated in the calibration report. This will allow us to use the calibrated sensitivity as a reference value for future calculations.

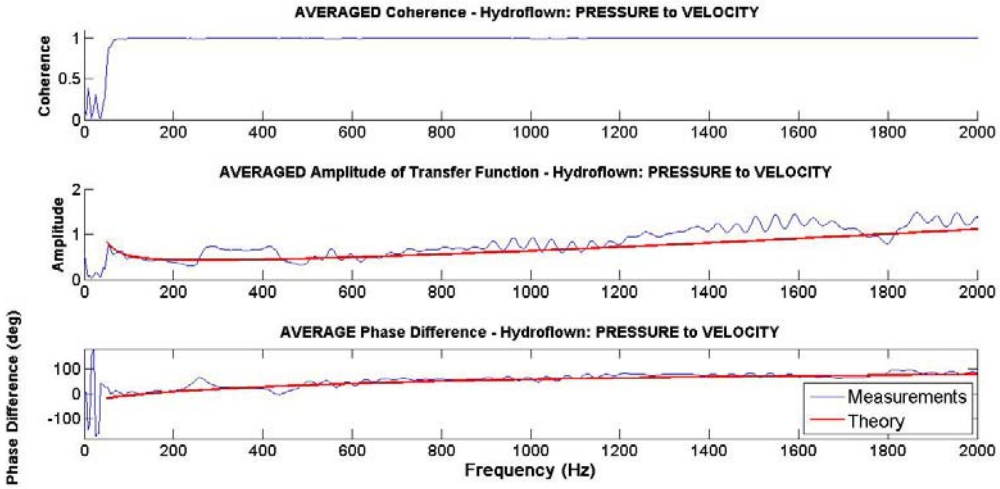

Figure 2. Plot of transfer function for the Microflown PU Match

C. BEAM PATTERN

1. Method

To determine the beam pattern of the particle velocity element, the Microflown PU match was attached to a Brüel & Kjær Turntable system and only the output of the particle velocity element was recorded. A Philips compression driver was fixed to a pole at 2.04 m. This time the ACO Pacific reference microphone was not installed. A Stanford RS preamplifier was used for amplification and filtering. Pre-amplification was set to 10x and a 1 kHz High pass and 100 kHz Low pass filter was used to reduce noise. An Agilent Waveform Generator was used to produce 1000 Hz, 1500 Hz and 2000 Hz CW signals at 1.0 V_{pp}.

The turntable conducted 360 degrees rotations with 6 degrees overshoot on both sides to ensure a continuous rotation speed during a complete circle. Data was acquired using National Instruments Labview and processed using Mathworks Matlab software.

2. The Result

During the experiment it became apparent that the vibrations of the turntable had a considerable effect on the experiment. Using a high pass filter at 1 kHz and measuring the beam pattern with frequencies above 1 kHz reduced this noise to acceptable levels.

The polar plot in Figure 3 shows the normalized response at 2 kHz over a 360° rotation. Although a frequency of 2 kHz produced the clearest results, all three frequencies showed the expected figure eight beam pattern provided in the data sheet.

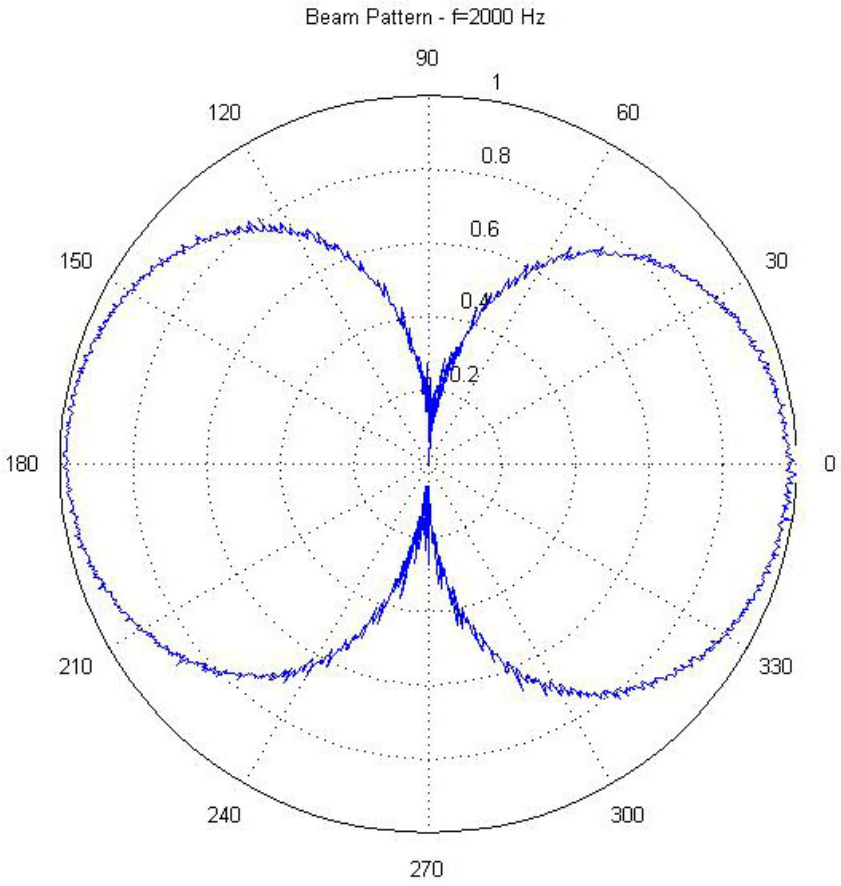

Figure 3. The beam pattern of the Microflown Titan in air

THIS PAGE INTENTIONALLY LEFT BLANK

III. SELECTION OF THE MATERIALS USED FOR ENCAPSULATION

A. INTRODUCTION

The Microflown Titan velocity sensor element uses two uncoated platinum filaments to measure the flow vector. Since the conducting filaments are uncoated they cannot be used in direct contact with seawater. To use the Microflown PU match underwater it therefore needs to be encapsulated. This encapsulation will affect the propagation of sound by reflection and refraction. Since this study is interested in both sound intensity and direction, it is important that the capsule has as a minimal influence on both these properties.

The capsule in which the sensor will be placed consists of two basic parts; the outer shell and the filling fluid. For the outer shell both the material and the shape will determine the effect on sound transmission and direction. The filling fluid needs to be non-conducting and have an impedance close to that of average seawater. Other selection criteria were the cost and availability. Since the goal of the study is to determine the feasibility to develop an underwater vector sensor based on Microflown technology, it was considered acceptable and efficient to work with materials with less than optimal properties.

The capsule was designed and produced at the NPS by J. Adeff. This chapter will explain the choices made in the design and some of the challenges during manufacturing.

B. THE OUTER SHELL

The shell was constructed using Devcon Flexane 80 urethane. This material is readily available and often used for hydrophones. The capsule has the shape of a cylinder with a hemispherical end cap (see Figure 4 and Figure 5). This guarantees a uniform shell thickness to all sides. Furthermore it ensured equidistance to the center axis from all sides.

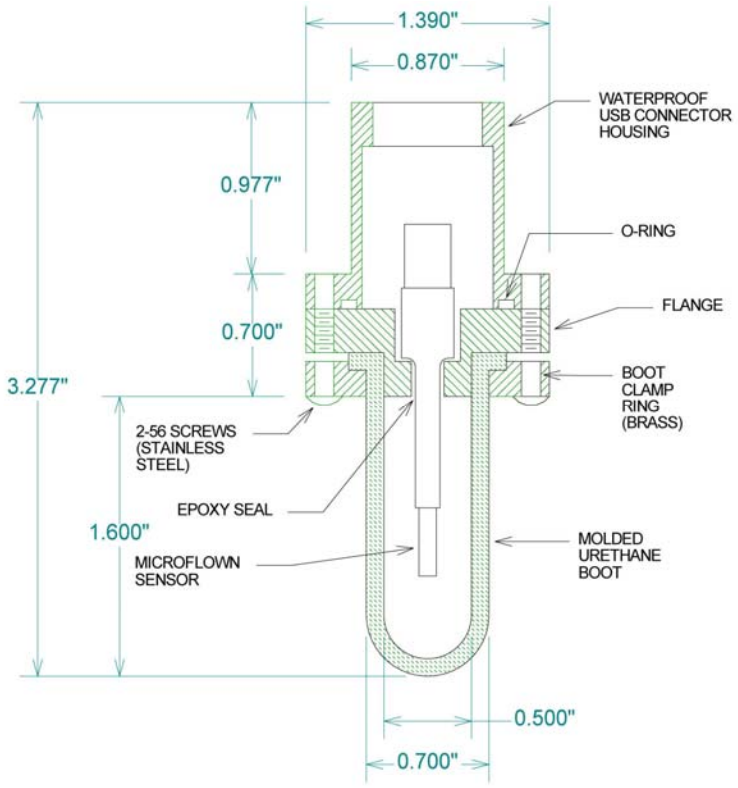

Figure 4. Capsule (designed by Jay Adeff)

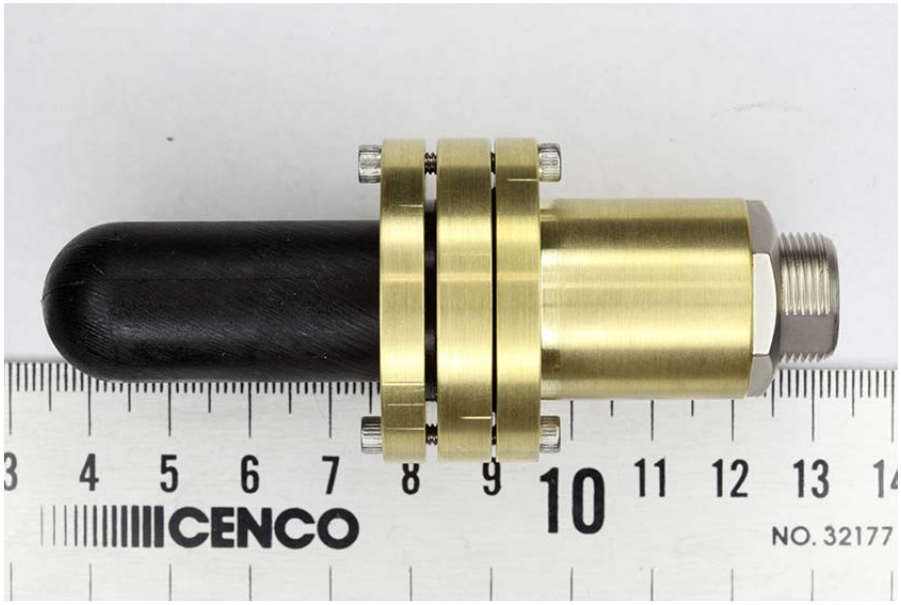

Figure 5. Complete encapsulated sensor along cm scale

C. THE FILLING FLUID

Castor oil, Baker DB grade, is widely used in hydrophones because of its excellent acoustic properties and compatibility with other transducer materials [7]. Furthermore, this castor oil is readily available at limited cost. Figure 6 shows how the characteristic impedance of castor oil (Baker DB grade) matches the characteristic impedance of seawater. Over the entire range of $0^{\circ}\text{C} - 25^{\circ}\text{C}$ the impedance mismatch is $< 10\%$.

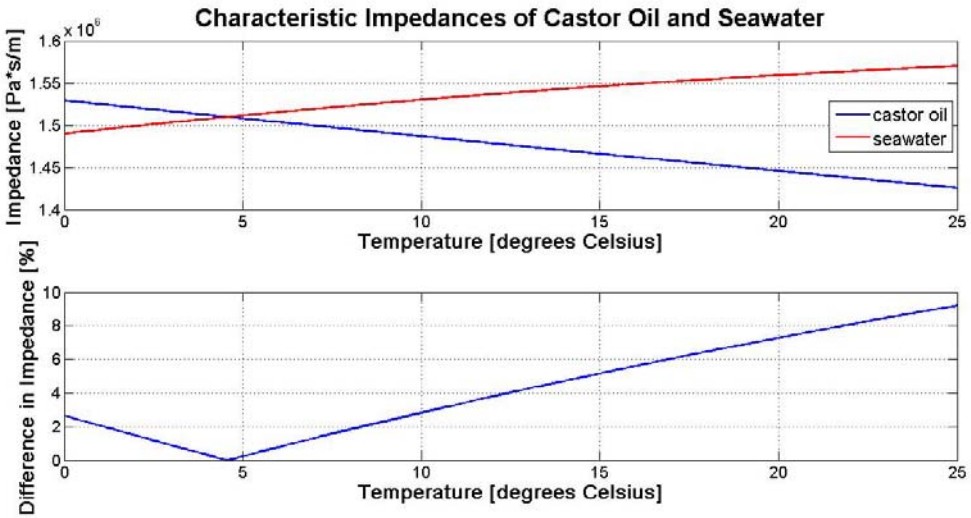

Figure 6. Impedance match of castor oil and seawater

D. SOME CRITICAL ADAPTATIONS

The current Microflown Titan sensor element has been designed for use in air only. The sensor uses platinum filaments at temperatures around $400^{\circ}C$ to optimize performance. The physical properties of a liquid can be very different from a gas. For instance the liquid has a boiling point at which bubbles will appear. This will greatly decrease the sensor performance and probably reduce the life cycle. For castor oil, the boiling point is $313^{\circ}C$ at atmospheric pressure. Due to increased heat transfer the Titan sensor element will operate at a slightly lower temperature than in air (the power provided to the sensor will remain the same), it will still be close to and probably over the boiling point of our filling fluid. To prevent bubbles from appearing, the operating

temperature needs to be considerably under the boiling point. Furthermore the platinum used in the filaments operates as a catalyst in the dissociation of the oil. This will not only produce anomalies as the chemical composition of the oil changes, but it will also cause a honey-like residue on the filaments themselves. This can be prevented by coating the filaments by a thin layer of quartz [8].

IV. THE PERFORMANCE UNDERWATER

A. INTRODUCTION

Now that composition of the prototype is known, a prediction of its performance can be made. In order to do this some assumptions and estimates have to be made. When empirical data becomes available these can be validated or corrected.

The first and most important part of predicting the performance of the sensor underwater is to estimate how the thermodynamic properties of the filling fluid will affect the heat distribution. Particle displacements due to sound waves are much smaller in a liquid than in a gas. The density of a liquid is much greater than that of a gas, so a lot more molecules are available to transfer the heat. Furthermore the heat capacities of the two media are very different. On the other side, the diffusion speed needs to remain large compared to the forced convection caused by the sound wave, so that the influence of the particle displacement due to the sound wave can be treated as a small alteration to the temperature profile. The start of the prediction is therefore to calculate how all these factors influence the performance.

The second part of the prediction is to estimate how the capsule will affect the performance. What reflection losses are expected as sound travels through the shell and then through the filling fluid? Is it possible to estimate the way that sound direction will be altered by refraction?

This chapter will first address the influence of the filling liquid on the performance of the Microflown Titan velocity sensor. Thereafter the influence of the packaging will be estimated. The conclusion will be an estimate of the sensor performance underwater. This will then be compared to empirical data in order to verify theory.

B. THE PERFORMANCE PREDICTION IN CASTOR OIL

1. The Temperature Difference between the Two Filaments

The sensitivity of the Microflown sensor is based on the temperature difference that occurs when a flow passes two heated filaments. The temperature can be calculated using the heat equation

$$\rho c_p \left(\partial_t T + \mathbf{v}\nabla \mathrm{T}\right) - k\nabla^2 T = Q, \tag{4}$$

where

$\rho =$ Density

$c_p =$ Specific heat

$T =$ Temperature

$k =$ Thermal conductivity

$Q =$ Generated heat

The temperature difference will create a difference in the resistance of the wires. The change in resistance is therefore a measure for the flow rate. A detailed calculation of the temperature difference between the wires due to sound waves can be found in [9]. There, the term $\mathbf{v}\nabla \mathrm{T}$ (the convective term in Equation (4)) is treated as a perturbation, because in air the diffusion speed is large compared to the forced convection. An important parameter is the heat diffusion coefficient $D = k / \rho c_p$. For air at $400^{\circ} C$ (the operating temperature of the Titan sensor element in air) $D_{air} \approx 6.5 \cdot 10^{-5} m^2 s^{-1}$. For castor oil at $313^{\circ} C$ (the maximum operation temperature in castor oil) $D \approx 3.2 \cdot 10^{-8} m^2 s^{-1}$. In the current sensor, with a distance between the wires (a) of 100 microns, the ratio between the forced convection (v) and the diffusion speed (D/a) at $SPL \approx 140 dB$ re $1 \mu Pa$ compares as

$$\frac{v_{air}}{D_{air}/a} = 3.14 \cdot 10^{-2} \ll 1 \text{ and } \frac{v_{castor\_oil}}{D_{castor\_oil}/a} = 2.39 \cdot 10^{-2} \ll 1$$

This shows that when the sensor operates in castor oil the diffusion speed is still much larger than the forced convection. This implies that the convective term can still be treated as a perturbation if the sensor is evaluated in oil.

Including the effect of the heat capacity of the sensors, the temperature difference is given by [9]

$$\Delta T = e^{i2\pi\bar{f}} \frac{2va}{D} \frac{P}{2\pi k l_y} \frac{1}{i\bar{f}_a} \times \frac{1-\sqrt{i\bar{f}_a}K_1\left(\sqrt{i\bar{f}_a}\right)}{1-i\frac{f}{f_{hc}}\left[K_0\left(\sqrt{i\bar{f}_L}\right)-K_0\left(\sqrt{i\bar{f}_a}\right)\right]}, \tag{5}$$

where:

$$\bar{f} = \frac{f}{f_D}$$

f = Frequency $[Hz]$

$$f_D = \frac{D}{2\pi a^2}$$

$$\bar{f}_x = \frac{2\pi f x^2}{D}$$

$$f_{hc} = \frac{D}{2\pi L h}\frac{\left(\rho c_p\right)_{air}}{\left(\rho c_p\right)_{sensor}} = \text{Second corner frequency}$$

h = Thickness of the filament

k = Thermal Conductivity Coefficient $\left[\frac{W}{m\cdot K}\right]$

l_y = Length of the wire $[m]$

v = Particle velocity $\left[\frac{m}{s}\right]$

P = Power $[W]$

$a =$ Distance between wires $[m]$

$L =$ Width of the filament

$K_1(x) =$ Modified Bessel function of the second kind of order 1

The frequency f in the first term, as stated in the article, was replaced by the dimensionless frequency $\overline{f}$, assuming that it was an error in the article. This change will not impact the resulting analysis of ratios as this term drops out. Calculating the ratio $\frac{\Delta T_{air}}{\Delta T_{oil}}$ will eliminate constant parameters from the equation, reducing uncertainty with regards to their values. Since the sensitivity is proportional to the temperature difference between the wires, this ratio can be used to scale the sensitivity function and thus predict the performance. The ratio can be broken down to

$$\frac{\Delta T_{air}}{\Delta T_{oil}} = \frac{k_{oil}}{k_{air}} \frac{v_{air}}{v_{oil}} \times \left\{ \frac{1-\sqrt{i\overline{f}_{a(air)}} K_1\left(\sqrt{i\overline{f}_{a(air)}}\right)}{1-\sqrt{i\overline{f}_{a(oil)}} K_1\left(\sqrt{i\overline{f}_{a(oil)}}\right)} \frac{1-i\frac{f}{f_{hc}}\left[K_0\left(\sqrt{i\overline{f}_{L(oil)}}\right)-K_0\left(\sqrt{i\overline{f}_{a(oil)}}\right)\right]}{1-i\frac{f}{f_{hc}}\left[K_0\left(\sqrt{i\overline{f}_{L(air)}}\right)-K_0\left(\sqrt{i\overline{f}_{a(air)}}\right)\right]} \right\} \tag{6}$$

In order to compare the performance in air to the performance in castor oil the calculations will be based on the same amount of acoustic intensity. The ratio between particle speed amplitudes (v) will therefore be based on the same IL.

2. The Total Sensitivity Response

The total frequency response of the Microflown can be approximated by [9]

$$|\Delta T| = \Delta T(0) \frac{1}{\sqrt{1+\frac{f^2}{f_{hc}^2}}} \frac{1}{\sqrt{1+\frac{f^2}{f_d^2}}}, \tag{7}$$

where

$f_d =$ Apparent corner frequency $=$ some arbitrary scaling factor $* \frac{D}{a^2}$, and

$$\Delta T(0) = \frac{va}{D}\frac{P}{2\pi k l_y}\left(\ln\left(\frac{\pi a}{2l_y}\right)+0.577\right).$$

This approximation will make it much easier to model the frequency response. Since $|\Delta T|$ is proportional to the actual response of the Microflown, the performance of the sensor in castor oil can be predicted by calculating the ratio $\frac{|\Delta T|_{air}}{|\Delta T|_{oil}}$. This yields

$$\frac{|\Delta T|_{air}}{|\Delta T|_{oil}} = \frac{D_{oil}}{D_{air}}\frac{v_{air}}{v_{oil}}\frac{k_{oil}}{k_{air}}\frac{\sqrt{1+\frac{f^2}{f_{hc\_oil}^2}}}{\sqrt{1+\frac{f^2}{f_{hc\_air}^2}}}\frac{\sqrt{1+\frac{f^2}{f_{d\_oil}^2}}}{\sqrt{1+\frac{f^2}{f_{d\_air}^2}}}. \tag{8}$$

Using this ratio, the expected performance of the encapsulated Microflown Titan sensor is shown in Figure 7.

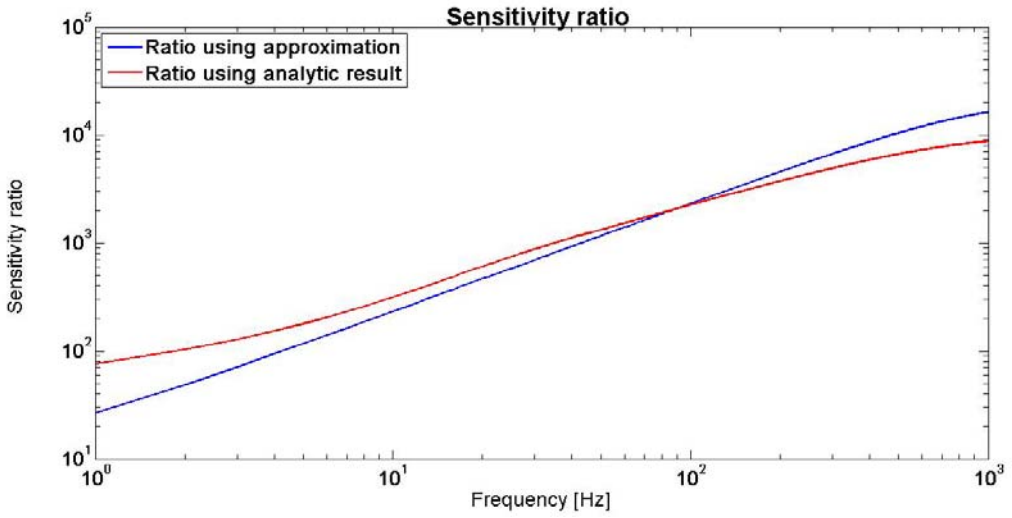

Figure 7. The sensitivity ratio in castor oil at 313° C

Figure 8 shows that the sensitivity ratio of the Microflown Titan element in castor oil at $313^{\circ}C$. At frequencies $>100Hz$ the approximation predicts less sensitivity in

castor oil than the analytic result of the temperature difference ratio. At $1000Hz$ the sensitivity ratio predicted by the approximation is twice the sensitivity predicted by the analytic result.

To be able to predict the response, the calibrated sensitivity in air is needed. The calibration report provides a graph of the sensitivity and a formula to calculate it. In the preceding section the sensor response in air was confirmed to agree with this formula. Figure 8 shows the calibrated sensitivity of the Microflown PU match in air as calculated from this formula prior to encapsulation.

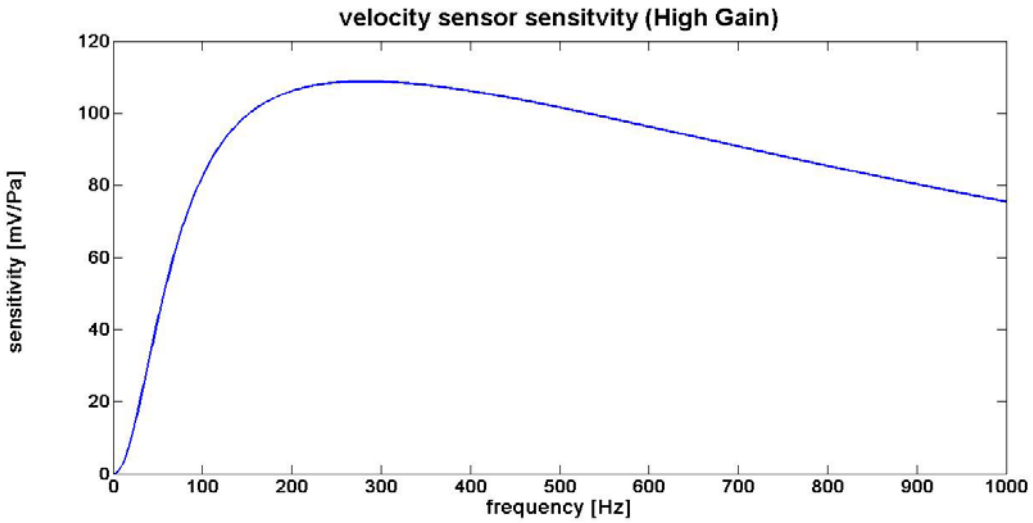

Figure 8. Sensitivity in air based on calibration report

Since the comparison of the sensitivity in air and castor oil is calculated and the sensitivity in air is known, we can predict the sensitivity in castor oil by:

$$Sensitivity_{castor\_oil} = \frac{Sensitivity_{air}}{Ratio|\Delta T|}. \tag{9}$$

3. The Reflection Losses

Reflection and refraction will occur due to the impedance mismatch. In the case of the encapsulated Microflown sensor in seawater, sound has to travel through three types of medium before reaching the Titan sensor element. Sound will first travel through

the seawater, then encounter the Flexane 80 urethane shell of the capsule. The sound then travels through the shell and enters the castor oil to propagate to the sensor element. At each boundary some portion of the sound is reflected and the direction of the sound is altered. Although the changes in apparent direction of sound are obviously important in a vector sensor, this thesis will not address this.

The impedance of seawater is well documented and the impedance of castor oil is also well known. The impedance of Flexane 80 urethane is not known. However, the shell has a very small thickness (d) compared to the wavelengths (λ) on the bandwidth of interest. Even at $1000Hz$ the ratio $\frac{d}{\lambda} < 0.01$, and can therefore be considered transparent.

The intensity transmission coefficient is given by [10]

$$T_I = \frac{4r_2 r_1}{\left(r_2 + r_1\right)^2}, \tag{10}$$

where $r_x = \rho_x c_x =$ characteristic acoustic impedance of the medium.

The measurements at NUWC were conducted in seawater at 20 degrees Celsius. At that temperature

$$r_{seawater} = 1.559 \cdot 10^6 \frac{Pa \cdot s}{m},$$

$$r_{Castor\_oil} = 1.446 \cdot 10^6 \frac{Pa \cdot s}{m}.$$

Therefore, $T_I = 0.999$, which means that the intensity of the sound is reduced by only 0.1% before the sound reaches the sensor element. For the comparison of the experimental results with the theoretical model, therefore, reflection losses can be neglected.

4. The Predicted Performance of the Encapsulated Sensor

Using the calibration report and the performance ratios, the predicted performance can be calculated.

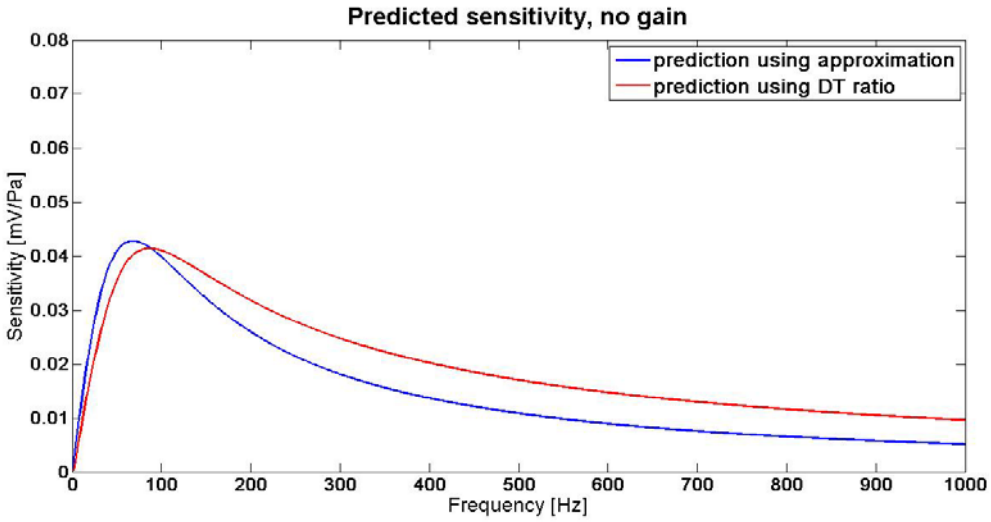

Figure 9. The predicted performance of the encapsulated sensor

Figure 9 displays the predicted performance of the encapsulated sensor. Comparing the prediction to the calibration report shows that the expected sensitivity is far less. Furthermore it shows that the capsule is expecting to shift the peak sensitivity to a lower frequency. The sensitivity of the encapsulated sensor drops off more quickly as the frequency increases.

At NUWC, experiments will be conducted to determine the actual sensitivity of the encapsulated sensor. The results of the experiments will be compared to the predicted sensitivity in castor oil to verify the theory. If the theory is confirmed, it can be used to determine sensor adaptations to increase its performance underwater.

V. COMPARING THE MEASUREMENTS TO THE PREDICTED PERFORMANCE

A. INTRODUCTION

At NUWC, two sets of measurements were done using the encapsulated Microflown PU match. These measurements were some done a few weeks apart. During the first set, responses at two different orientation angles were determined, separated by 45 degrees. First the measurements were executed along the presumed axis of maximum response. Thereafter, the same measurements were executed at an orientation of 45 degrees to the assumed axis of maximum response. In the second set of measurements, only single orientation measurements were done. The single orientation measurements were intended to correspond to the maximum response axis of the particle velocity sensor. The aim of the measurements was to determine the responses at various Sound Pressure Levels (SPLs) and to determine if the sensor still exhibited its directionality between the two measurement angles.

B. UNCERTAINTIES

The nature of the sensor causes some very significant uncertainties when analyzing its performance. First, the operating temperature is not exactly known. In air, the filaments are heated to approximately $400^{\circ}C$. The larger heat conduction in castor oil will reduce that temperature because the power applied will remain the same. Since the boiling point of castor oil is $313^{\circ}C$ at standard atmospheric pressure, this will be assumed to be the temperature at which the encapsulated Microflown PU match will operate. Bubbles appearing at the filaments when the castor oil starts to boil will further influence the experimental results in an unpredictable way.

Second, the platinum will act as a catalyst in the dissociation of the castor oil [8]. This process will leave a honey-like residue on the wires, reducing the sensitivity over time. This process is expected to influence the measurements within hours of operation.

Finally, the exact angle of refraction is not known, because the impedance of the Flexane 80 shell is not known. More importantly, due to its small size, the precise

orientation of the Titan sensor element within the capsule is very hard to determine. Since the Microflown PU match has a classic figure eight beam pattern, this will influence its apparent sensitivity when insonified at oblique angles.

C. THE EXPERIMENTAL SETUP

Figure 10. Experiment setup at NUWC

The experiments to determine the sensitivity of the encapsulated Microflown PU match were conducted at NUWC by John Whitacre (NUWC staff). The most important part of the experiments was to determine the sensitivity of the sensor when a source was located along the axis of maximum response. To determine if the encapsulated sensor retained its directionality, the sensor was also placed at a 45 degree angle to the initial orientation. During the experiments, the encapsulated sensor was submerged in an anechoic tank with a sound source and a well-known A47 SN 16 reference hydrophone. The bandwidth between $50-1000Hz$ was swept both linear and logarithmic at SPL's between $90-170dB$ re $1\mu Pa$. Below 110dB re $1\mu Pa$ however, the travelling field was

not created properly. During the experiment the temperature of the tank was $20^{\circ}C$. From the output voltage the sensitivity was calculated in dB re $1V/\mu Pa$. These values were provided for further analysis and comparison to the theory.

The theory suggests that the current encapsulated sensor will be very insensitive compared to its sensitivity in air. This means that the expected output voltage is very low, even when high amplitude sound is directed at the sensor. The results of the first set suggested that the sensor was indeed very insensitive. From the first set of data it seemed that the sensitivity of the sensor decreased as the SPL was increased. This could indicate that the sensor was being overdriven. To further examine this possibility, a second, much more elaborate set of experiments were conducted three weeks after the first set. In this set the SPLs were reduced in $3dB$ steps to $90dB$ re $1\mu Pa$. In total 45 measurements were conducted.

D. THE RESULTS OF THE SENSITIVITY TEST

The first test with a clear response was obtained in the first set, using a SPL of 140dB, no gain. This was the second experiment conducted with the sensor, so the effect of any residue on the wires should be small. This test will also be used to determine if the encapsulated sensor retains its directionality.

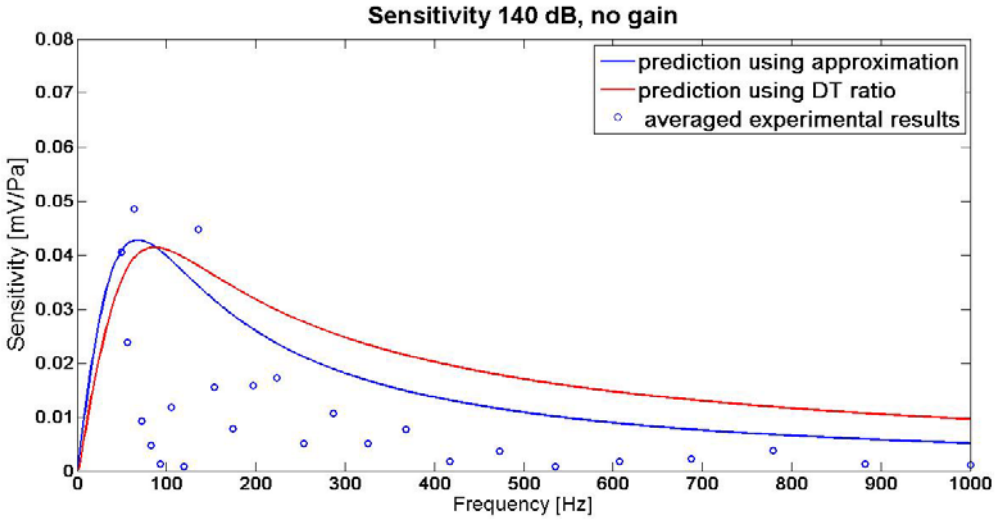

Figure 11. Sensitivity using 140dB, no gain

In Figure 11, the experimental sensitivity is plotted, together with the theoretical prediction using the approximation and using the ratio of analytic temperature differences. Clearly the encapsulated Microflown PU match is more sensitive to lower frequencies. The measurements show that the apparent sensitivity of the encapsulated sensor is highest around $60Hz$. It then shows an unexpected jumpy behavior in sensitivity throughout the measured bandwidth. On the other hand, the position of the peak sensitivity and the general envelope of the sensitivity seems to roughly correspond to our model.

Furthermore, in this case the approximation seems to predict the sensitivity somewhat better than the direct calculation using the ratio of the temperature differences. The difference between the approximation and the exact solution is shown in [9]. That the approximation appears to give a better prediction of the experimental results can be the result of a misalignment of the sensor in the capsule. The sensor has no calibrated direction markings on it. The small size makes it very hard to determine the exact straight angle to the sensor during the encapsulation process. Because the sensor is directional, any misalignment will result in a reduced sensitivity in a stationary experiment. A further error in the assessed reflection losses caused by the impedance mismatch can further influence the apparent sensitivity. However, none of these factors adequately explain the somewhat oscillatory behavior of the sensitivity and the influence of electronic noise or problems with the calibration process cannot be ruled out.

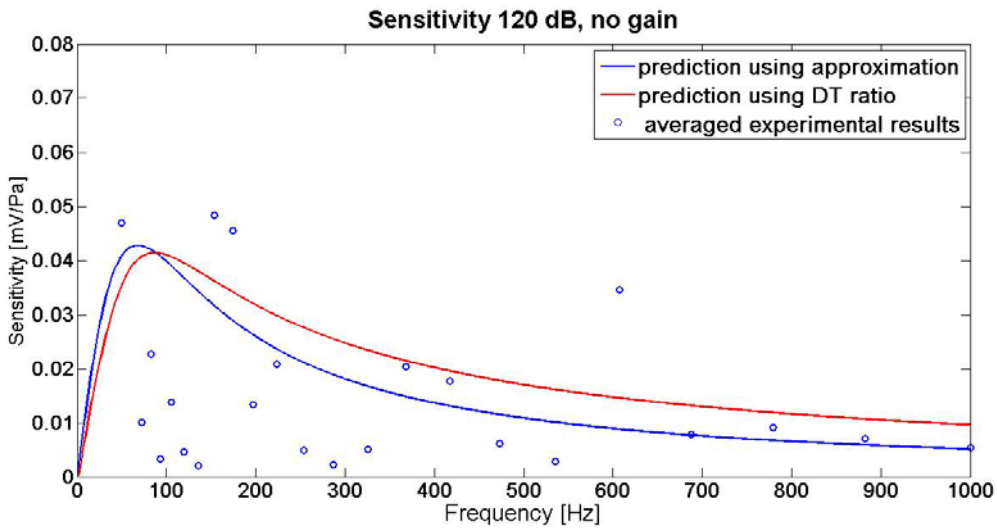

Figure 12. Sensitivity at 120dB, no gain

In Figure 12, the measured sensitivity is shown using SPL of $120dB$ re $1\mu Pa$ without gain. The sensitivity over the bandwidth changes in a similar way as with the SPL of 140dB re $1\mu Pa$ and again the irregular sensitivity is apparent.

Experiments conducted with SPL $<110dB$ re $1\mu Pa$ gave even more irregular results. Sensitivity seemed to randomly vary at different SPLs. Additional experiments showed that the traveling field was not created well at pressure levels $<110dB$ re $1\mu Pa$ .Since the acoustic particle velocity cannot be inferred from the reference hydrophone when the contributions of the standing wave components are unknown, these experiments could not be used.

To better understand the sensitivity of the encapsulated Microflown PU match in comparison with the model, all experimental data for SPL $>110dB$ re $1\mu Pa$ were converted to their values without any gain and then averaged.

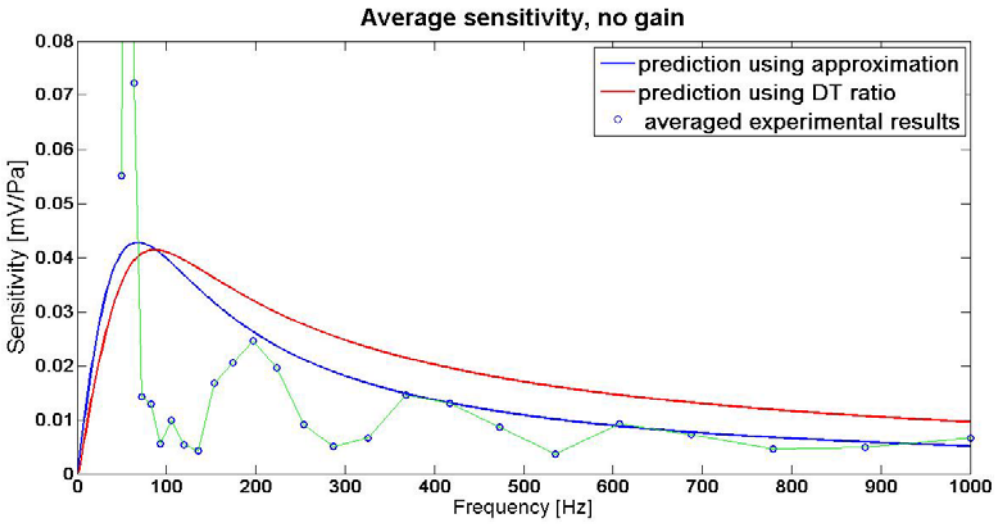

Figure 13. Averaged sensitivity without gain

The averaged results are shown in Figure 13, together with the predictions based on the approximation and the calculated temperature difference ratio. This averaging over eight experiments at SPLs $110-160dB$ re $1\mu Pa$ shows a strong peak greater than the expected value around 60Hz followed by clear oscillatory behavior.

This behavior could be caused by electronic noise. If $60Hz$ and subsequent harmonics are the reason for the periodicity in the sensitivity, the peaks and lows would correspond with a harmonic frequency of $60Hz$. The initial peak is in between $56Hz$ and $64Hz$. This suggests that it is caused by electronic noise. In Table 1 the difference between the peaks and lows from the averaged experimental data and the $60Hz$ harmonics is shown. The percentage difference seems to imply great coherence between the harmonics and the peaks and lows. However, the step size during these experiments was logarithmic. This means that the step size started with $4Hz$ and increased over the bandwidth to $110Hz$. The peaks/lows at higher frequencies are therefore determined less precisely than the peaks/lows at low frequencies. To investigate this variation further, the raw output voltage of the measurement at $140dB$ and $120dB$ re $1\mu Pa$ were compared. Based on the $20dB$ re $1\mu Pa$ difference in SPL, a factor of 10 was expected in the ratio of output voltages. However, Figure 14 shows that the actual output voltage ratio was only about 3 and then highly fluctuating over the bandwidth. The output

voltage on the reference microphone showed the same fluctuations. Inspection of the traveling wave tube showed that, at the time of the experiments, the projector might not have been functioning properly. Therefore, it is justified to assume that, besides traveling wave components, also some standing wave components were present in the tube. The impact of the introduction of standing wave components is unclear since the system's feedback mechanism for generating traveling waves is unknown. However, as the system sweeps through frequency, the large fluctuations observed on the reference hydrophone strongly suggest issues with the desired system response. Unfortunately time constraints prevented repeating the experiment in a re-calibrated tube.

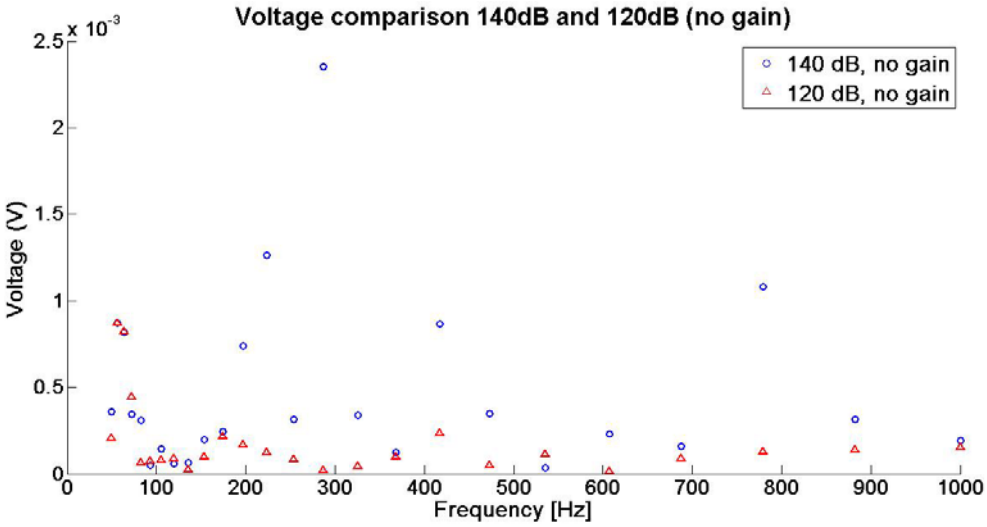

Figure 14. Output voltage comparison

Further investigation to determine the cause of the periodicity in the sensitivity is needed.

60 Hz harmonic	peak	low	% difference
60 Hz	56.7 Hz		6%
120 Hz		135.7 Hz	12%
180 Hz	197.4 Hz		9%
300 Hz		287 Hz	5%
360 Hz	368.4 Hz		2%
540 Hz		535.7 Hz	1%
600 Hz	606.7 Hz		1%

Table 1. Comparison peaks/lows to 60Hz harmonics

E. RESULTS OF THE DIRECTIONALITY TEST

To determine if the encapsulated sensor retains directionality, a set of measurements were conducted with the sensor at a 45 degree angle relative to the initial angle. Although the exact refraction angle is not known, a 45 degree angle should show a significant drop in sensitivity at all frequencies. To determine if this was the case, all experiments at SPL $>110dB$ re $1\mu Pa$ measured at 45 degrees were averaged and compared to the averaged sensitivity of the same SPLs for the initial orientation. The averaging was done over four data sets at both angles.

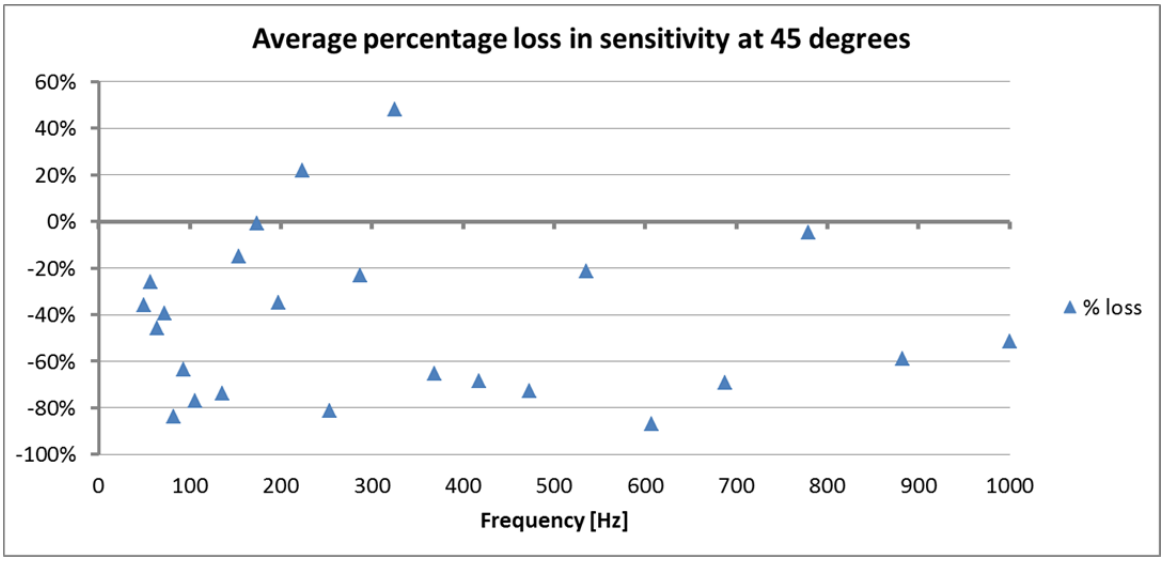

Figure 15. Average percentage of sensitivity loss at an angle of 45 degrees

The results of the comparison are shown in Figure 15. Although the percentage loss varies over the bandwidth, it is obvious that overall the sensitivity is considerably lower after a rotation of 45 degrees from the presumed axis of maximum response. Therefore, it can be concluded that the encapsulated sensor retains directivity. The average loss was about 45%. The expected drop in sensitivity would be 30% from the measured beam pattern (see Figure 3). The difference could be due to additional reflection losses. An alternative cause is that the initial alignment was not precisely along the maximum response axis. If instead the two measurements were at angles 30 degrees and 75 degrees relative to the maximum response axis (and 45 degrees relative to one another), then this drop in sensitivity would not be unexpected. The variation of the drop in sensitivity, however, is significant and cannot be explained by a constant misalignment. This could again indicate that the traveling wave was not entirely the same at the position of the Microflown during the experiments at the two orientation angles. To determine the actual beam pattern, additional measurements are needed, where the angle is changed with small increments and more data sets are gathered.

F. EXPERIMENTAL CONCLUSION

The data shows that the encapsulated sensor is able to detect sound underwater. The envelope of the sensitivity roughly agrees with predictions using the calibrated sensitivity in air and the calculated sensitivity ratio or the proportional ratio in temperature differences between the filaments. The oscillations in the sensitivity are not predicted by the theory and need additional measurements to investigate. Calibration problems in the traveling wave tube might explain some periodicity in the apparent sensitivity of the Microflown Titan sensor element. Electronic noise seems to have influenced measurements around $60Hz$. Further research is needed to determine its contribution to the apparent sensitivity at higher frequencies. The encapsulated sensor retains directionality. Additional measurements are needed to establish the exact beam pattern.

VI. EFFECTS OF SENSOR MODIFICATIONS

A. INTRODUCTION

The performance of the Microflown Titan is determined by the difference in temperature between the filaments as a result of a passing sound wave. A higher operating temperature will increase the sensitivity. As previously stated, in air the operating temperature of the Microflown Titan sensor element is approximately $400^{\circ}C$. The boiling point of castor oil is $313^{\circ}C$ at standard atmospheric pressure. Bubbles appearing when the liquid starts to boil will greatly reduce its performance. It is therefore important to operate the velocity sensor element at temperatures below the boiling point. Flow studies using hot wire anemometry by H. Eckelmann have indicated that a temperature of about half the boiling point will make the effect of bubbles appearing insignificant [8]. Since the sensor will be used underwater, increased pressure will increase the boiling point and therefore also increase the optimum operating temperature.

The higher impedance of both seawater and castor oil compared to air will result in a much decreased particle displacement and velocity caused by sound of the same Intensity Level (IL). The amount of molecules available per unit volume to carry heat from one filament to another however is much larger in castor oil than in air. These parameters translate directly into the optimal distance apart at which the filaments should be placed.

In this chapter, the results of varying both the operating temperature of the filaments and the distance between the wires will be evaluated. This can be used to determine these parameters in a next prototype with the goal of improving performance.

B. THE METHOD

At all times the reference performance will be the Microflown Titan sensor as was encapsulated. This sensor, when used in air, has an operating temperature of approximately $400^{\circ}C$ and a distance between the wires of $100\mu m$. These values will not change throughout this chapter.

Several performance determining parameters are temperature dependent. The first step in predicting the performance of the sensor over a temperature range is therefore to approximate the values of these parameters over that temperature range. This was done by curve fitting data points using Microsoft Excel 2010 for the specific heat (c_p) and thermal conductivity (k). This approximation was necessary because only sparse data was available. A formula to calculate the density and sound speed in castor oil was taken from [7]. To achieve different temperatures, the power (P) needs to become variable. From the power in the current sensor, the electric current $\left(I_0\right)$ can be calculated. Assuming $\left(I_0\right)$ to be constant and using

$$P = I_0^2 R, \tag{11}$$

and

$$R = R_0 \alpha \left(\Delta T\right), \tag{12}$$

we obtain

$$P = I_0^2 R_0 \alpha \left(\Delta T\right), \tag{13}$$

with

$\alpha = 3.93 \cdot 10^{-3} C^{-1} =$ temperature coefficient,

$I_0 = 9.9 \cdot 10^{-2} A =$ current through the filament.

The resulting formulas were integrated in Equations (5) and (7). To then calculate the ratios of the temperature difference and sensitivity response, Equations (6) and (8) were altered to be able to use a constant value for a in air and a varying value for a in castor oil. In Figure 16 and Figure 17 the specific heat and thermal conductivity are shown. Only two data points were available to determine the thermal conductivity of castor oil. The approximation was acceptable, however, because the total change over the entire temperature range was $< 6\%$ and consistent with similar oil types.

The approximated relationships will be treated as valid over the arbitrary temperature range $40^{\circ}C - 400^{\circ}C$, even though the boiling point of castor oil will make these approximations invalid. We can do this, because in our comparisons only the temperatures below the boiling point are used.

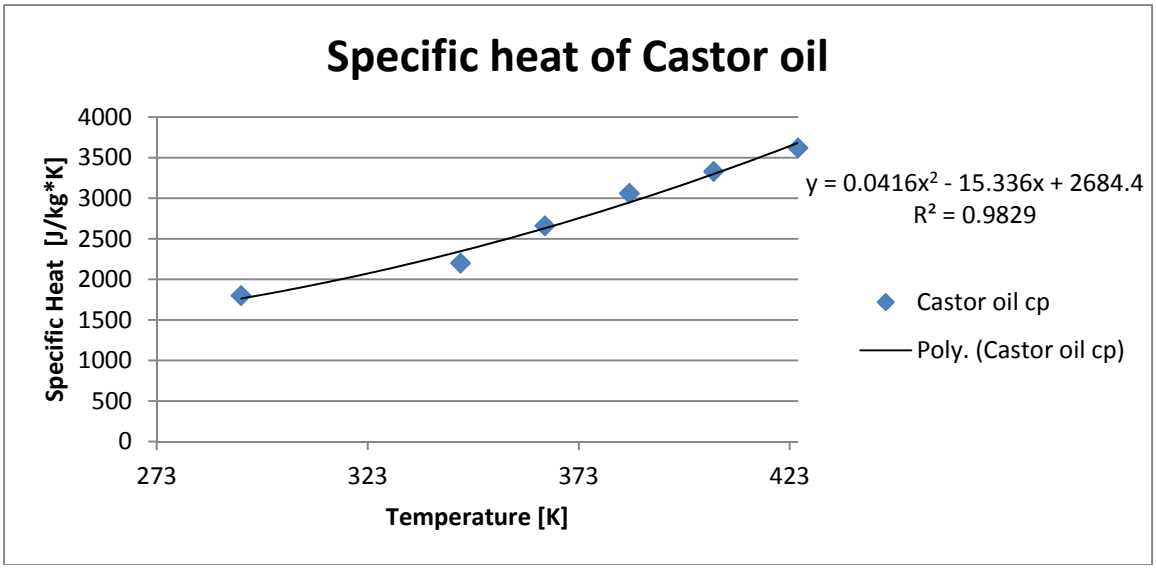

Figure 16. Specific heat of castor oil

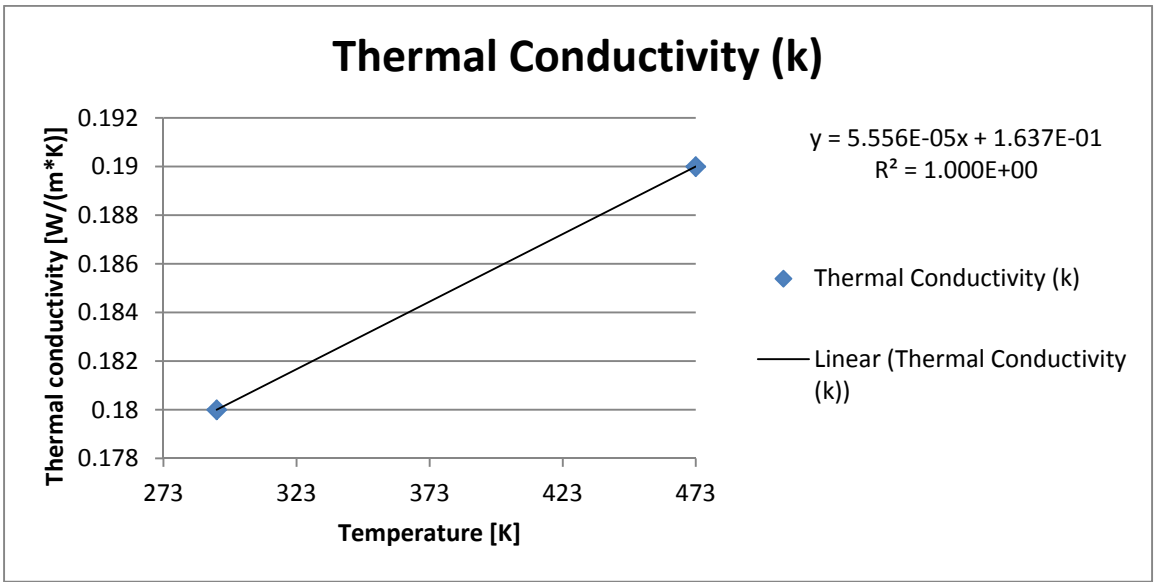

Figure 17. Thermal conductivity of castor oil

The temperature difference ratio now becomes

$$\frac{\Delta T_{air}}{\Delta T_{oil}} = \frac{k_{oil}}{k_{air}} \frac{P_{air}}{P_{oil}} \frac{v_{air}}{v_{oil}} \times \left\{ \frac{1 - \sqrt{i\bar{f}_{a(air)}} K_1\left(\sqrt{i\bar{f}_{a(air)}}\right)}{1 - \sqrt{i\bar{f}_{a(oil)}} K_1\left(\sqrt{i\bar{f}_{a(oil)}}\right)} \frac{1 - i\frac{f}{f_{hc}}\left[K_0\left(\sqrt{i\bar{f}_{L(oil)}}\right) - K_0\left(\sqrt{i\bar{f}_{a(oil)}}\right)\right]}{1 - i\frac{f}{f_{hc}}\left[K_0\left(\sqrt{i\bar{f}_{L(air)}}\right) - K_0\left(\sqrt{i\bar{f}_{a(air)}}\right)\right]} \right\}, \quad (14)$$

while the sensitivity approximation ratio becomes

$$\frac{|\Delta T|_{air}}{|\Delta T|_{oil}} = \frac{D_{oil}}{D_{air}} \frac{v_{air}}{v_{oil}} \frac{P_{air}}{P_{oil}} \frac{k_{oil}}{k_{air}} \frac{\sqrt{1 + \frac{f^2}{f_{hc\_oil}^2}}}{\sqrt{1 + \frac{f^2}{f_{hc\_air}^2}}} \frac{\sqrt{1 + \frac{f^2}{f_{d\_oil}^2}}}{\sqrt{1 + \frac{f^2}{f_{d\_air}^2}}}. \quad (15)$$

Using Equations (14), (15) and (9) with temperature dependency incorporated for the castor oil parameters, the effect of altering the operating temperature and the distance between the wires can be predicted. The experimental results have confirmed that the sensitivity in air can be scaled to the sensitivity in castor oil at a different operating temperature. This will be used to determine the sensitivity of the encapsulated sensor at operating temperatures $40^\circ - 313^\circ C$ at any given distance between the wires.

C. THE EFFECTS OF VARIATIONS IN OPERATING TEMPERATURE AND DISTANCE BETWEEN THE WIRES

The temperature dependence of the sensitivity of the current encapsulated sensor is shown in Figure 18. The peak of the current sensitivity is $0.04\ mV/Pa$ at 85Hz and at $313^\circ C$. The sensitivity deteriorates with increasing frequency and with decreasing operating temperature.

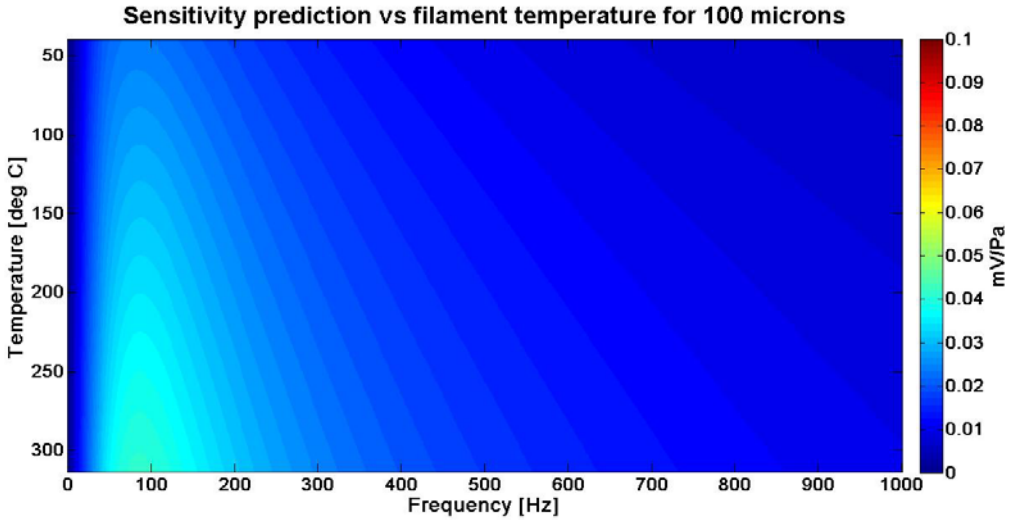

Figure 18. Temperature and frequency dependence of the sensitivity at 100 microns

Reducing the distance between the wires will decrease the sensitivity at very low frequencies. However, the sensitivity will be increased at higher frequencies [11]. The crossover point of the encapsulated sensor is $< 5Hz$, so that sensitivity is in general increased (see Figure 19).

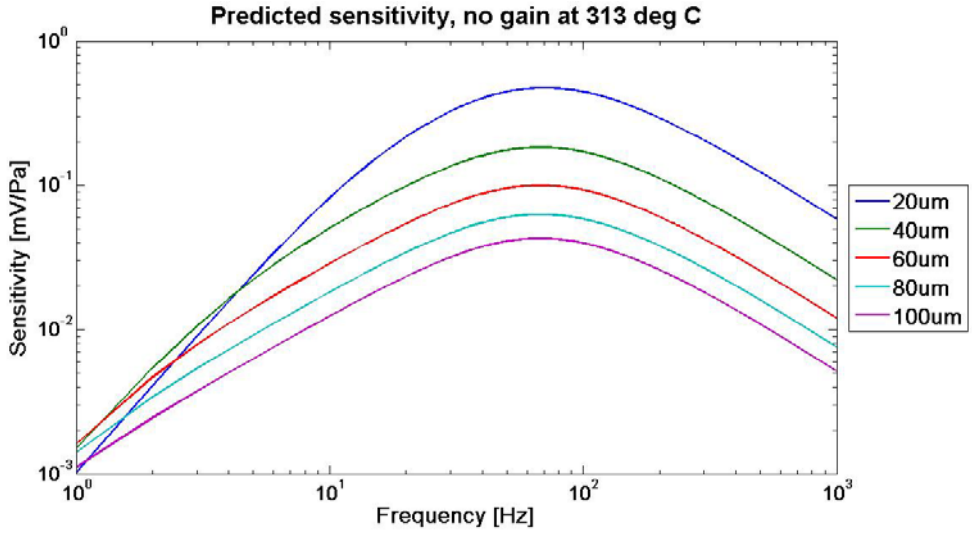

Figure 19. Sensitivity at $313^{\circ}C$ and 20µm, 40µm, 60µm, 80µm and 100µm

The distance between the wires cannot be decreased indefinitely, however. The sensor is based on two filaments through which a current flows. As the distance between

the wires decreases, the induced magnetic fields and electric forces will start to obstruct proper performance. At what distance this will start to occur is not part of this thesis. However, the minimum distance will be assumed to be $\geq 20\mu m$. Castor oil and quartz (possible material for coating the platinum filaments) are very good insulators with dielectric constants of 4.7 and 3.8, respectively, at room temperature.

Lowering the temperature will also lower the sensitivity over the whole frequency range (see Figure 18). Still, it is necessary to investigate the sensitivity at lower temperatures in order to prevent decreased performance by dissociation and/or boiling of the castor oil. The temperature at which the oil is free of boiling is dependent on the pressure and therefore the operating depth of the sensor. Finding the exact temperature at which dissociation stops is not a part of this thesis. Studies in this field by H. Eckelmann [8] however, suggest that below half the boiling temperature, dissociation becomes insignificant. For castor oil therefore, an optimum operating temperature lies somewhere between $100^{\circ} - 200^{\circ} C$ at standard atmospheric pressure.

The combined effect of variation of the operating temperature and the distance between the filaments is shown in Figures 20–22. The effects start to significantly alter sensitivity at $< 40\mu m$ between the filaments.

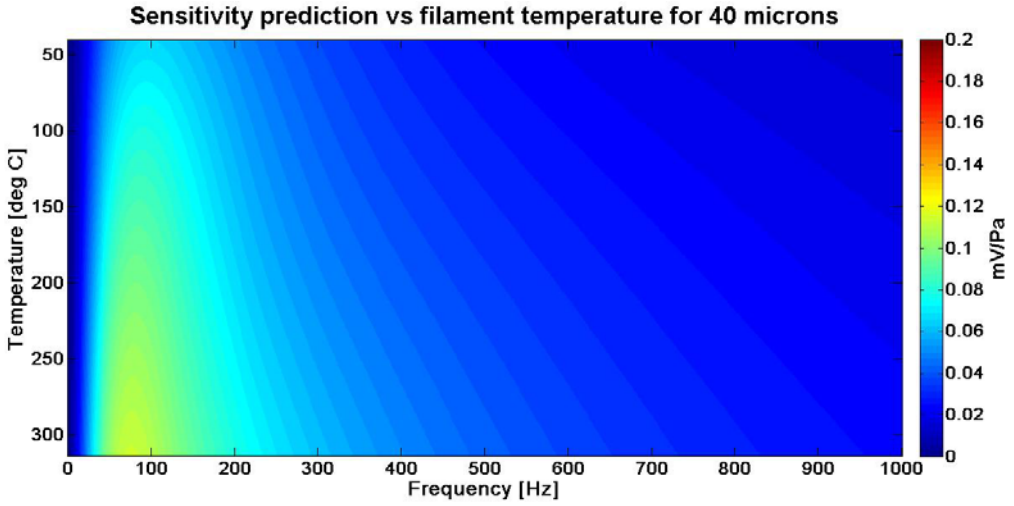

Figure 20. Temperature and frequency dependence of the sensitivity at 40 microns

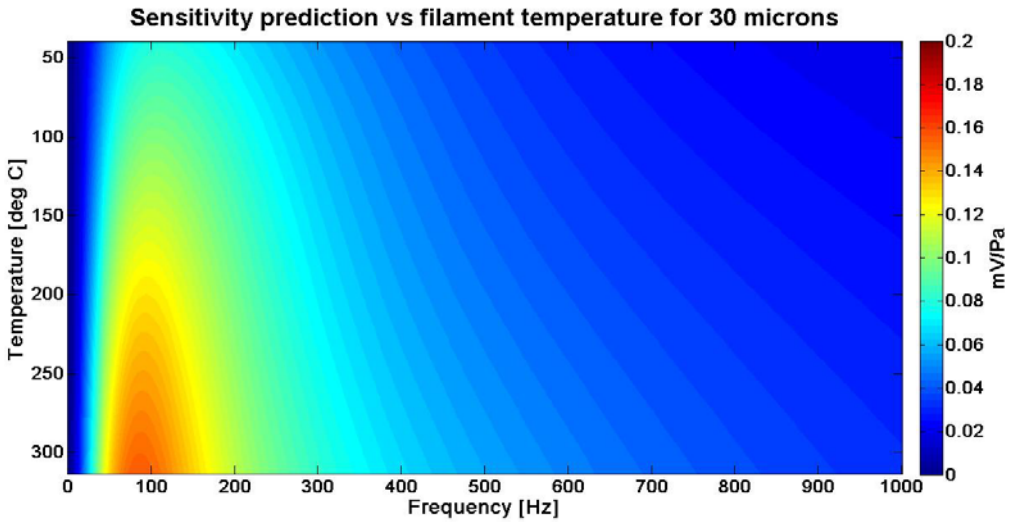

Figure 21. Temperature and frequency dependence of the sensitivity at 30 microns

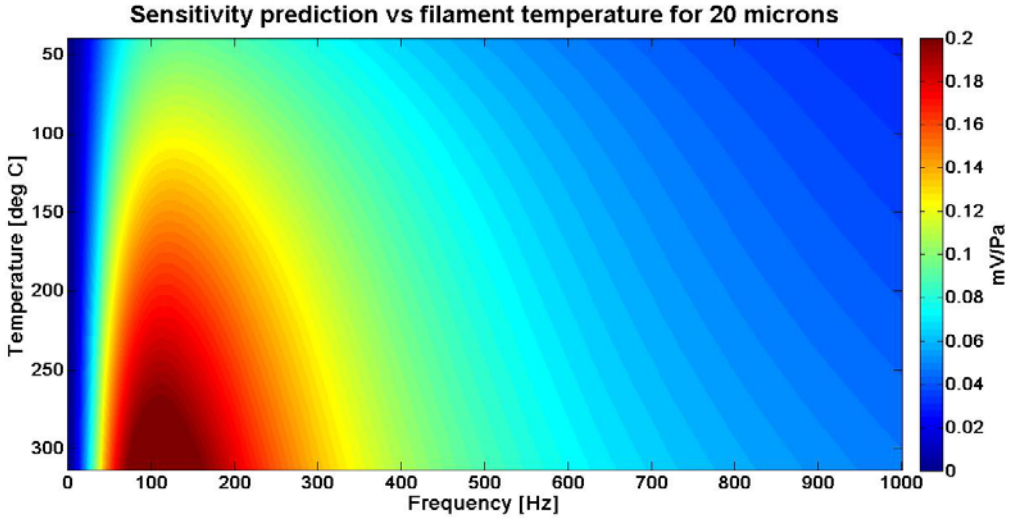

Figure 22. Temperature and frequency dependence of the sensitivity at 20 microns

For $313^{\circ}C$ and $200^{\circ}C$ the effect of changing the distance between the wires is shown in Figures 23 and 24, respectively.

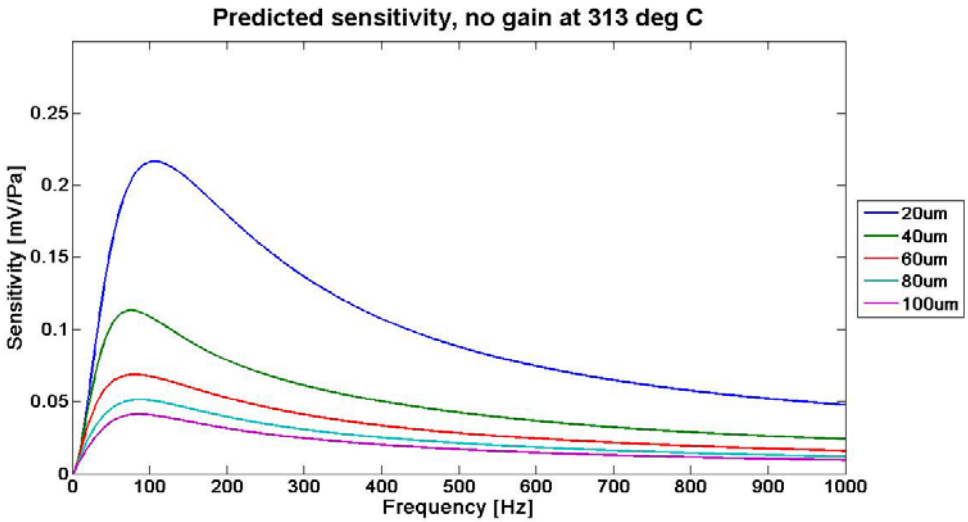

Figure 23. Distance dependence of the sensitivity at $313^{\circ}C$

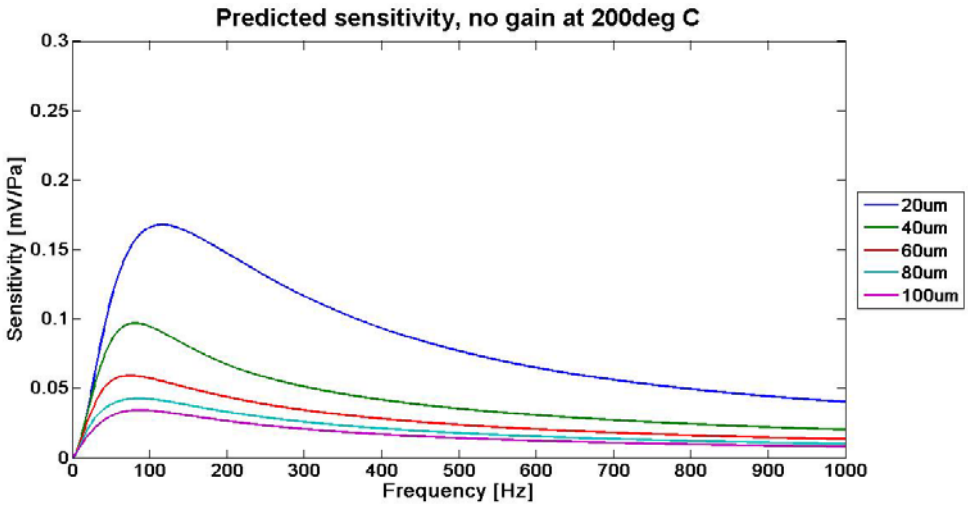

Figure 24. Distance dependence of the sensitivity at $200^{\circ}C$

From Figures 23 and 24 it can be concluded that decreasing the distance between the wires has a much larger effect than changing the temperature in the ranges of interest. Based on ratio of the temperature differences between the wires, decreasing the distance between the filaments to $40\mu m$ will result in a $8dB$ gain in sensitivity at both $313^{\circ}C$ and $200^{\circ}C$. Decreasing the distance to $20\mu m$ will result in a $14dB$ gain for both temperatures. A filling fluid with similar impedance and with a much higher boiling point might improve this gain even further.

According to the theory, decreasing the distance between the filaments will increase sensitivity rapidly as the distance between the wires gets very small. This raises the question as to whether the theory still holds at distances $< 30\mu m$ or whether other influences become dominant. If the theory does hold, it would be useful to establish the minimum distance apart that can be achieved.

The sensitivity peaks just below $100Hz$ in the region where the spikes were observed during the experiments with the current sensor. If the sensor is already sensitive in this region, reducing the distance between the wires might increase sensitivity to the point that the sensor is overdriven. In that case, a design with two sensor elements could be considered. One sensor element optimized for frequencies $< 150Hz$ and one optimized for higher frequencies. Since the sensitivity peak does not shift very far as the distance between the wires decreases it is not necessary to add more sensor elements. The size of the elements (only a few millimeters) enables stacking them without any significant increase in overall sensor size.

D. LIMITS IN FILAMENT PROXIMITY

Although theory suggests that a reduction of the distance between the wires will increase the sensitivity significantly, technological restrictions will limit the extent to which the wires can be brought together. J.W. van Honschoten has experimented in air with filaments set $30\mu m$ apart [9]. It therefore seems reasonable to assume that sensors with a distance between the filaments of about $30\mu m$ can be produced.

E. SENSOR MODIFICATION CONCLUSIONS

Reducing the distance between the wires increases the sensitivity significantly. Reducing the operating temperature will have a relatively small negative effect on the sensitivity. Reducing the operating temperature in castor oil and coating the filaments is necessary to avoid boiling and dissociation of the castor oil. Literature indicates that this effect is negligible when the operating temperature is reduced to about $200^{\circ}C$. The effect of reducing the distance between the wires increases as the filaments are closer together.

This encourages experiments to determine the validity of the underlying theory at these distances. In future designs of the sensor a stacking of two elements could be considered if the sensor is found to be too sensitive at low frequencies.

VII. CONCLUSION AND RECOMMENDATIONS

A. CONCLUSIONS

It seems feasible to adapt the Microflown PU match for underwater use. Experiments seem to indicate that the theories to predict its performance hold when the sensor is submerged in oil. However, the oscillations of the measured sensitivity and the high peak in measured sensitivity around $60Hz$ are not predicted by our model and need further investigation. The influence of the calibration error in the experimental set up and the influence of electronic noise need to be determined.

Based on its acoustic and electric properties, castor oil is a good choice as a filling fluid. Additional gain can be achieved by finding a more stable filling fluid with similar or better acoustic and electric properties, but a much higher boiling point. Operating the sensor in a liquid instead of a gas will require some adaptations to the sensor. The operating temperature needs to be well below the boiling point of the oil. Coating the filaments will be necessary to overcome catalytic effects of the platinum wires. Further strengthening of the wires may be required to prevent damage when operating in a much denser medium.

At the current distance between the filaments, sensitivity underwater is low. Decreasing the distance between the filaments will increase the sensitivity over the whole bandwidth of interest. A gain of $14-21dB$ could be achieved if the distance between the wires is reduced to $20-40\mu m$. Reducing the operating temperature to $200^{\circ}C$ does not significantly reduce sensitivity at these distances.

The encapsulated sensor retains a level of directivity. The exact beam pattern needs to be determined in future research.

B. RECOMMENDATIONS FOR FUTURE DESIGN

The next prototype should have coated filaments to prevent the platinum from acting as a catalyst in the dissociation of the oil. The operating temperature needs to be well below the boiling point of the inert liquid of choice. Based on its acoustic properties

castor oil is a good filling fluid for the capsule. In this case an operating temperature of $200^{\circ}C$ is advised. The wire distance should be reduced to $< 40\mu m$ in order to improve sensitivity.

C. RECOMMENDATIONS FOR FUTURE RESEARCH

Future research is necessary to investigate the oscillations in the sensitivity. The conducted experiments should be repeated in a re-calibrated traveling wave tube to determine if standing wave components are the cause of the periodicity in the sensitivity. Additional experiments are necessary to determine the influence of electronic noise. Subsequent research is necessary to determine if the beam pattern of the encapsulated sensor maintains its proper response. Finally, it needs to be determined if the current prediction model will hold at very small distances between the wires.

APPENDIX A. LIST OF EQUIPMENT

Equipment and settings used during all measurements	
Microflown PU match consisting of: - Microflown Titan acoustical particle velocity sensor - Knowles FG series miniature sound pressure transducer	Frequency range: - Velocity sensor: 0.1 Hz–20 kHz - Pressure sensor: 20 Hz–20 kHz
Microflown Technologies MFSC-2 2 channel signal conditioner	- Gain set to 'High' - Correction mode set to 'Off'
Post-processing: Mathworks Matlab Version 2010a	
Additional equipment and settings used to determine beam pattern	
Agilent type 33220A Arbitrary Waveform Generator	- 1000 Hz, 1500 Hz, 2000 Hz CW - V_{pp} set to '1.0 V'
Brüel & Kjær Turntable system type 9640	
Stanford RS preamplifier model SR560	Pre-amplification: 10x High pass filter: 1 kHz Low pass filter: 100 kHz
Philips compression driver	
Data acquisition software: National Instruments Labview 2011	Sampling frequency: 25 Hz
Additional equipment and software used to determine transfer function	
National Instruments Compact DAQ USB chassis model NI 9172	
National Instruments Sound and Vibration DAQ module model NI 9234 (2 total)	

Austin AU-15G Amplifier	- Overdrive set to 'ON' - Volume set to 'MAX'
Hewlett Packard Function Generator model 33120A	- Mode: White Noise - Amplitude: $10V_{pp}$
ACO Pacific Calibrated Pressure microphone model 7046	
ACO Pacific ½" pre-amplifier model 4012	
Data acquisition software: - Mathworks Matlab 2011 - Data acquisition toolbox	
Additional equipment and software analyze data NUWC	
Microsoft Excel 2010	

APPENDIX B. EVALUATION OF THE MICROFLOWN IN AIR

A. THE FULL EVALUATION

The proper functioning of the Microflown PU Match sensor and all its sensor elements was confirmed. To be able to do this, first the transfer function was established between the pressure element and the velocity element. Also the transfer function with an independent and well known ACO Pacific model 7046 microphone was established and compared to the initial results. Finally the Noise Spectrum Level (NSL) was determined.

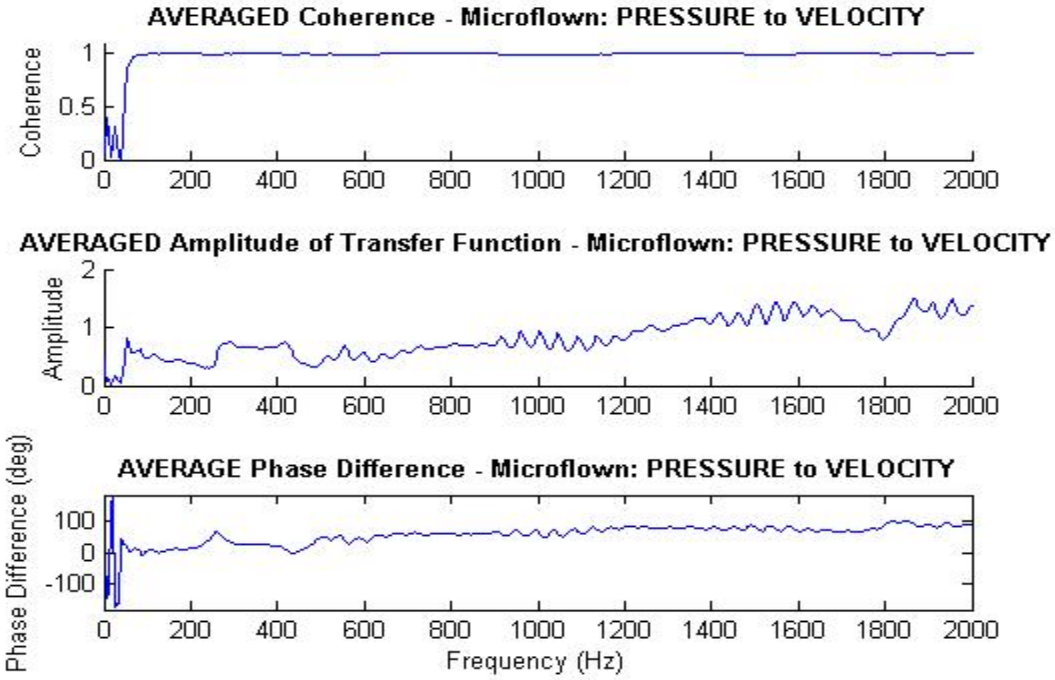

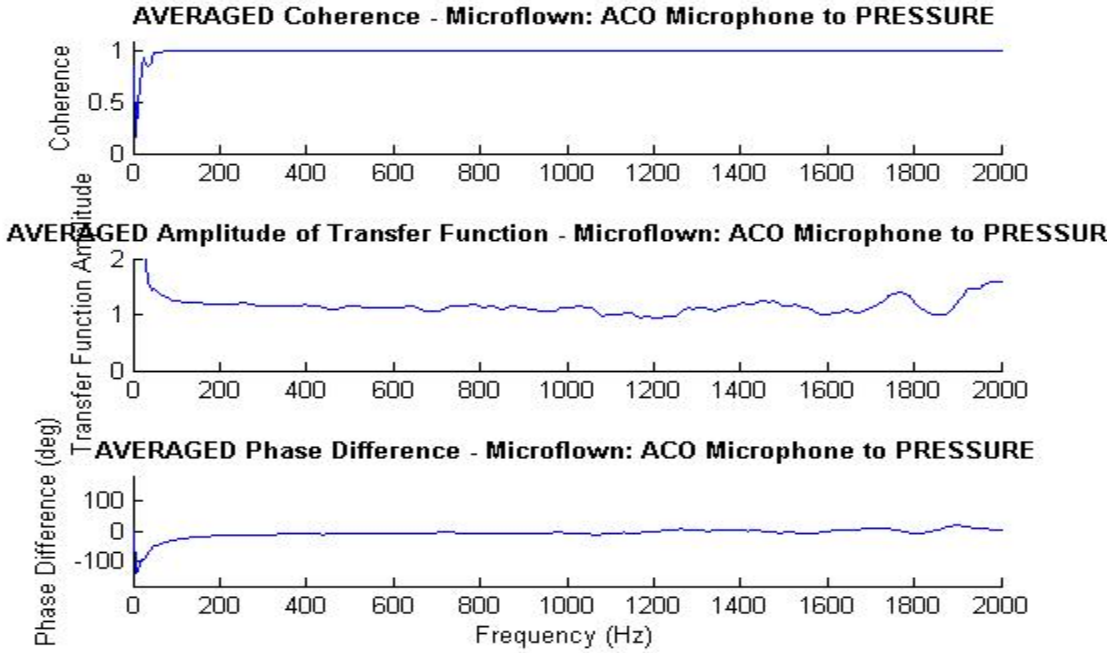
AVERAGED Coherence - Microflown: ACO Microphone to PRESSURE
Coherence
AVERAGED Amplitude of Transfer Function - Microflown: ACO Microphone to PRESSUR
Transfer Function Amplitude
AVERAGED Phase Difference - Microflown: ACO Microphone to PRESSURE
Phase Difference (deg)
Frequency (Hz)

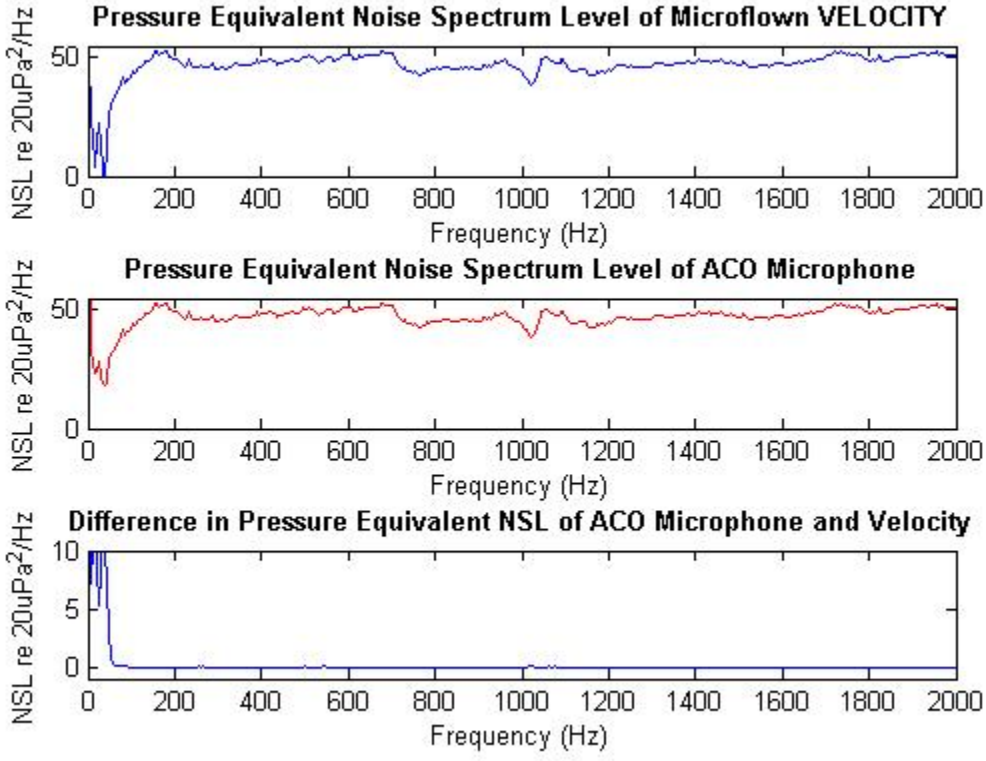
Pressure Equivalent Noise Spectrum Level of Microflown VELOCITY
NSL re 20uPa2/Hz
Frequency (Hz)
Pressure Equivalent Noise Spectrum Level of ACO Microphone
Difference in Pressure Equivalent NSL of ACO Microphone and Velocity

B. THE MATLAB CODE FOR THE TRANSFER FUNCTION

```
%% Hydroflown Transfer Function
% Program to read in Hydroflown data and compute transfer function between
% pressure sensor and velocity sensors
%
%% Clean up
clear all
clc
close all
%% Setting up FFT
maxchan = 6;            %maximum number of data channels captured
numpass = 250;          %number of loop iterations in vi sampling routine
N = 1024;               %number of samples per channel per pass
M = numpass * N;        %total sample length per channel
Fs = 4267;              %sampling freq
NFFT = 2^10;
overlap = NFFT/2;
window = hanning(NFFT);

%% Channel Designation
prs1 = 1; % sensor 324 pressure
blu1 = 2; % sensor 324 blu velocity
grn1 = 3; % unused
prsR = 4; % ACO pressure
prs2 = 5; % unused
blu2 = 6; % unused

Sref1 = prs1;   % hydroflown Pressure Channel
Sref2 = blu1;   % hydroflown Velocity Channel

plotsensor='Microflown';
plotref1='PRESSURE';
plotref2='VELOCITY';
```

```
%% Loading Datasets


bindata = zeros(M,maxchan); %initialize matrix to allocate memory


datasets = 3;   %number of data sets for averaging


for ds=1:datasets  %cycle through number of data sets


    if ds == 1

        bindata =
importdata('C:\Users\Marnix\Documents\MATLAB\Thesis\measurements\Mar20_WN_10Vpp_max
_1_60s.mat');

    else if ds == 2

            bindata =
importdata('C:\Users\Marnix\Documents\MATLAB\Thesis\measurements\Mar20_WN_10Vpp_max
_2_60s.mat');

        else if ds == 3

                bindata =
importdata('C:\Users\Marnix\Documents\MATLAB\Thesis\measurements\Mar20_WN_10Vpp_max
_3_60s.mat');

            end

        end

    end


    bindata = bindata';         %change to row data




    %% Computation for Transfer Function for Sound Probe Pressure to velocity
channel

    gamma_p2v(:,ds) =
mscohere(bindata(Sref1,:),bindata(Sref2,:),window,overlap,NFFT,Fs);

    [P2V(:,ds),F] = cpsd(bindata(Sref1,:),bindata(Sref2,:),window,overlap,NFFT,Fs);

    [V(:,ds),F] = pwelch(bindata(Sref2,:),window,overlap,NFFT,Fs);

    [P(:,ds),F] = pwelch(bindata(Sref1,:),window,overlap,NFFT,Fs);

    Hp2v(:,ds) = P2V(:,ds)./V(:,ds);   %  PRESSURE to Velocity
```

```
    %% Computation for ACO Reference to Pressure element channel

    gamma_pACO(:,ds) =
mscohere(bindata(prsR,:),bindata(Sref1,:),window,overlap,NFFT,Fs);

    [P2ACO(:,ds),F] =
cpsd(bindata(prsR,:),bindata(Sref1,:),window,overlap,NFFT,Fs);

    [P(:,ds),F] = pwelch(bindata(Sref1,:),window,overlap,NFFT,Fs);


    F2x(:,ds) = P2ACO(:,ds)./P(:,ds);   % ACO to PRESSURE


end


    %% PLOT Transfer functions

    % VELOCITY element to PRESSURE element Transfer Function

    figure(1)

    subplot(3,1,1)

    hold on

    plot(F,gamma_p2v(:,1),'b')

    ylabel('Coherence')

    title(['Coherence - ',plotsensor,': ',plotref1,' to
',plotref2],'FontWeight','bold')

    axis([0 2000 0 1.1])


    subplot(3,1,2)

    hold on

    plot(F,abs(Hp2v(:,1)),'b')

    ylabel('Transfer Function Amplitude')

    title(['Amplitude of Transfer Function - ',plotsensor,': ',plotref1,' to
',plotref2],'FontWeight','bold')

    axis([0 2000 0 2])


    subplot(3,1,3)

    hold on

    plot(F, rad2deg(angle(Hp2v(:,1))),'b')

    title(['Phase Difference - ',plotsensor,': ',plotref1,' to
',plotref2],'FontWeight','bold')

    ylabel('Phase Difference (deg)')
```

```
    xlabel('Frequency (Hz)')

    axis([0 2000 -180 180])


    % PLOT averaged VELOCITY element to PRESSURE element Function

    figure(2)

    subplot(3,1,1)

    hold on

    gamma_p2v=sum(gamma_p2v,2)/3;

    plot(F,gamma_p2v,'b')

    ylabel('Coherence','FontSize',14)

    title(['AVERAGED Coherence - ',plotsensor,': ',plotref1,' to
',plotref2],'FontSize',18,'FontWeight','bold')

    axis([0 2000 0 1.1])


    subplot(3,1,2)

    hold on

    Hp2v = sum(Hp2v,2)/3;

    plot(F,abs(Hp2v),'b')

    ylabel('Amplitude','FontSize',14)

    title(['AVERAGED Amplitude of Transfer Function - ',plotsensor,': ',plotref1,'
to ',plotref2],'FontSize',18,'FontWeight','bold')

    axis([0 2000 0 2])


    subplot(3,1,3)

    plot(F, rad2deg(angle(Hp2v)),'b')

    title(['AVERAGED Phase Difference - ',plotsensor,': ',plotref1,' to
',plotref2],'FontSize',18,'FontWeight','bold')

    ylabel('Phase Difference (deg)','FontSize',14)

    xlabel('Frequency (Hz)','FontSize',14')

    axis([0 2000 -180 180])


    % PLOT PRESSURE element to ACO microphone Transfer Function

    figure(3)

    subplot(3,1,1)

    hold on
```

```
    plot(F,gamma_pACO(:,1),'b')

    ylabel('Coherence')

    title(['Coherence - ',plotsensor,': ACO Microphone to '
,plotref1],'FontWeight','bold')

    axis([0 2000 0 1.1])



    subplot(3,1,2)

    hold on

    plot(F,abs(F2x(:,1)),'b')

    ylabel('Transfer Function Amplitude')

    title(['Amplitude of Transfer Function - ',plotsensor,': ACO Microphone to '
,plotref1],'FontWeight','bold')

    axis([0 2000 0 2])



    subplot(3,1,3)

    hold on

    plot(F, rad2deg(angle(F2x(:,1))),'b')

    title(['Phase Difference - ',plotsensor,': ACO Microphone to '
,plotref1],'FontWeight','bold')

    ylabel('Phase Difference (deg)')

    xlabel('Frequency (Hz)')

    axis([0 2000 -180 180])



    % PLOT averaged PRESSURE element to ACO Transfer Function

    figure(4)

    subplot(3,1,1)

    hold on

    gamma_pACO=sum(gamma_pACO,2)/3;

    plot(F,gamma_pACO,'b')

    ylabel('Coherence')

    title(['AVERAGED Coherence - ',plotsensor,': ACO Microphone to '
,plotref1],'FontWeight','bold')

    axis([0 2000 0 1.1])



    subplot(3,1,2)
```

```
    hold on

    F2x = sum(F2x,2)/3;

    plot(F,abs(F2x),'b')

    ylabel('Transfer Function Amplitude')

    title(['AVERAGED Amplitude of Transfer Function - ',plotsensor,': ACO
Microphone to ' ,plotref1],'FontWeight','bold')

    axis([0 2000 0 2])



    subplot(3,1,3)

    hold on

    plot(F, rad2deg(angle(F2x)),'b')

    title(['AVERAGED Phase Difference - ',plotsensor,': ACO Microphone to '
,plotref1],'FontWeight','bold')

    ylabel('Phase Difference (deg)')

    xlabel('Frequency (Hz)')

    axis([0 2000 -180 180])



    % PLOT VELOCITY element to ACO microphone transfer function

    figure(5)

    subplot(2,1,1)

    FH=Hp2v.*F2x;  %transfer function to correct velocity to ACO pressure direct

    plot(F,abs(FH),'b')

    ylabel('Transfer Function Amplitude')

    title(['Amplitude of Transfer Function - ',plotsensor,': ACO Microphone to
',plotref2],'FontWeight','bold')

    axis([0 2000 0 3])

    subplot(2,1,2)

    plot(F,rad2deg(angle(FH)),'b')

    ylabel('Phase Difference (deg)')

    xlabel('Frequency (Hz)')

     title(['Phase difference of Transfer Function - ',plotsensor,': ACO Microphone
to ',plotref2],'FontWeight','bold')

    axis([0 2000 -180 180])



    %% Determine Noise Spectrum Level
```

```
     bindata = zeros(M,maxchan); %initialize matrix to allocate memory


   bindata =
importdata('C:\Users\Marnix\Documents\MATLAB\Thesis\measurements\Mar20_WN_10Vpp_max
_3_60s.mat'); %initialize matrix to allocate memory

    m=0.05433;  %aco sensitivity

    bindata = bindata';         %change to row data


 noise_signal = bindata(Sref2,:);

 noise_signal = noise_signal - mean(noise_signal);

 penf=pwelch(noise_signal,window,overlap,NFFT,Fs);

 penf=penf.*(FH.*conj(FH))/m^2*1E12/400;  %pressure equivalent noise floor
computation re 20uPa

 penf = 10*log10(penf);


ACO = bindata(prsR,:);

ACO = ACO - mean(ACO);

[PACO, F] = pwelch(ACO,window,overlap,NFFT,Fs);

PACO = PACO/m^2;  % ACO corrected to Pa

PACO = PACO*1E12/400;  % ACO signal in 20uPa

PACO = 10*log10(PACO);

diff=PACO-penf;




%% Plot Noise Spectrum Levels

% PLOT Noise Spectrum Level measured by ACO microphone and PRESSURE element

 figure(6)

 subplot(3,1,1)

 plot(F,penf,'b')

 xlabel('Frequency (Hz)')

 ylabel('NSL re 20uPa^2/Hz')

 title(['Pressure Equivalent Noise Spectrum Level of ',plotsensor,' '
plotref2],'FontWeight','bold')

 axis([0 2000 0 55])
```

```
 subplot(3,1,2)

 plot(F,PACO,'r')

 xlabel('Frequency (Hz)')

 ylabel('NSL re 20uPa^2/Hz')

 title('Pressure Equivalent Noise Spectrum Level of ACO
Microphone','FontWeight','bold')

 axis([0 2000 0 55])


 subplot(3,1,3)

 plot(F,diff,'b')

 hold on

%  plot(F,penf,'r')

 xlabel('Frequency (Hz)')

 ylabel('NSL re 20uPa^2/Hz')

 title('Difference in Pressure Equivalent NSL of ACO Microphone and
Velocity','FontWeight','bold')

 axis([0 2000 -1 10])
```

C. MATLAB CODE FOR DETERMINING THE BEAM PATTERN

```
%% Calculte beampattern on Microflown particle velocity sensor

% frequency 1500 Hz

% Sampling period 4.00e-2 s

clear;

clc

%

c1c=xlsread('2000_cropped_clean.xlsx');

tt=4.00e-2*length(c1c);             % total time [s]

c1c(:,1)=c1c(:,1)-c1c(1,1);         % start at t=0 s

amp=c1c(:,2);                       % define amp [V]

dbamp=20.*log10(amp);               % convert to decibels

dbamp=dbamp-min(dbamp);             % set minimum to 0 dB

dbamp=dbamp/max(dbamp);

angamp(:,1)=c1c(:,1)*((2*pi)/tt);   % convert time to radians

angamp(:,2)=dbamp;
```

```
polar(angamp(:,1),angamp(:,2));     % plot beampattern
title('Beam Pattern - f=2000 Hz');
```

THIS PAGE INTENTIONALLY LEFT BLANK

APPENDIX C. MATLAB CODE TO DETERMINE ACOUSTICAL PROPERTIES OF CASTOR OIL

```
%% Rho_0, c Calculation of Castor oil

% Intended to gain insight in the acoustic properties of castor oil and seawater as
a

% function of temperture

%% Clean up

clear

clc

close all

%% parameters

t=0:0.1:25;                          % Temperture range of the oil in deg Celcius

p=20.265;                             % Pressure in dBar

SA=35*ones(1,length(t));             % Salinity [g/kg] (constant in this case)

%% Calculation density and speed of sound Castor oil

rho=1000./(1.02714+7.04e-4.*t+9.66e-7.*t.^2+3.0e-9.*t.^3-4.91e-4*(p/100)-2.633e-
6*(p/100).*t-4.04e-9*(p/100).*t.^2-8.8e-11*(p/100).*t.^3+1.471e-6*(p/100)^2+9.2e-
9*(p/100)^2.*t.^2-3.63e-9*(p/100)^3-1.66e-11*(p/100)^3.*t);

c=1570*(1.000-2.15e-3.*t+4.0e-6.*t.^2+2.5e-6*(p/100).*t+2.22e-3*(p/100)-3.0e-
6*(p/100)^2);

%% Calculation density and speed of sound sea water

[rho_s] = gsw_rho_t_exact(SA,t,p);

[c_s]= gsw_sound_speed_t_exact(SA,t,p);

%% rho*c products

rho_c_c=rho.*c;                                    % Characteristic Impedance
Castor oil

rho_c_s=rho_s.*c_s;                                % Characteristic Impedance
Seawater

delta=((abs(rho_c_c-rho_c_s))./rho_c_s)*100;         % Difference in Impedance  [%]

%% Plot

figure (1)

subplot (2,1,1)

plot(t,rho)

hold on

grid on
```

```
plot(t,rho_s,'r')

xlabel('Temperture [degrees Celcius]')

ylabel('Density [kg/m^3]')

hleg1=legend('castor oil','seawater','Location','SouthWest');

title('Density and sound speed in Castor Oil and Seawater at
10m','FontWeight','bold')

subplot (2,1,2)

plot(t,c)

hold on

grid on

plot(t,c_s,'r')

xlabel('Temperture [degrees Celcius]')

ylabel('speed of sound [m/s]')

hleg1=legend('castor oil','seawater','Location','South');

figure(2)

subplot (2,1,1)

plot(t,rho_c_c)

hold on

grid on

plot(t,rho_c_s,'r')

xlabel('Temperture [degrees Celcius]','FontSize',16,'FontWeight','demi')

ylabel('Impedance [Pa*s/m]','FontSize',16,'FontWeight','demi')

hleg1=legend('castor
oil','seawater','Location','SouthWest','FontSize',16,'FontWeight','demi');

title('Characteristic Impedances of Castor Oil and Seawater at
10m','FontSize',20,'FontWeight','bold')

subplot(2,1,2)

plot(t,delta)

grid on

xlabel('Temperture [degrees Celcius]','FontSize',16,'FontWeight','demi')

ylabel('Difference in Impedance [%]','FontSize',16,'FontWeight','demi')
```

APPENDIX D. MATLAB CODE FOR PERFORMANCE PREDICTION

```
%% Sensitivity prediction

% Script determines the temperature differences between the wires for both air and
Castor oil based on the

% the formulae in the article by J.W. Honsbroek, “Analytic model of a two-wire
thermal

% sensor for flow and sound measurements).” It also models the

% approximation given in the articles. All parameters are made temperature

% dependent to predict performance over a wide range of temperatures.

%% Clean up

clear;

clc;

close all

format long

%% Basic parameters

f=0:1:1000;             % frequency range [Hz]

T=313:1:673;            % Temperature range [K]

TT=40:1:400;            % Temperature range in Celcius

TTT=673;                % approximate operating temperature (air) [deg C]

p=10.1325;              % Atmospheric Pressure in dBar

step=20e-6;             % step distance between wire [m]

v_a=0.02420;            % abitrary particle velocity (IL 78 dB re 1e-12 W/m^2 in
air) [m/s]

v_c=6.186e-06;          % Particle velocity (IL 78 dB re 1e-12 W/m^2 in Castor Oil)
[m/s]

[X Y]=meshgrid(f,T);

% Microflown

ly=0.001;               % Length of the filaments [m]

L=2e-6;                 % Estimated half width of the filament [m]

A=2e-10;                % Crosssection of a filament

I0=9.871e-2;            % Current based on P=12mW in air [A]

a_a=100e-6;             % distance between wire in the microflown Titan [m]
```

```
a_c=20e-6;              % initial (variable) distance between wire potential
hydroflown [m]

a_max=100e-6;           % maximum distance between wires

ns=a_max/step;          % Number of steps

h_pt=100e-9;            % thickness of platinum layer [m]

alpha=3.93e-3;          % Temperature coefficient of resistivity Platinum [C^-1]

h_SiNi=200e-9;          % thickness of SiNi layer [m]

rhoc_pt=2.85e6;         % density times specific heat Pt [J/(m^3*K)]

rhoc_SiNi=1.66e6;       % density times specific heat SiNi [J/(m^3*K)]

%% Pre-allocate matrices

ratio_FR=zeros(length(T),length(f));

ratio_DT=zeros(length(T),length(f));

FR_a=zeros(length(T),length(f));

pred1=zeros(length(T),length(f));

pred11=zeros(length(T),length(f));

%% Calculate Power to acomplish temperature

resist=3.675e-10*TT+9.93e-8;       % resistivity of Platinum

R0=resist*ly/A;                    % Resistance of the filaments over temperature

P=I0^2.*R0;

%% Calibration report

%% input parameters

% sensitivity

suh_250Hz=122.5;    % sensitivity (high gain) at 250Hz [mV/Pa]

sul_250Hz=0.9732;   % sensitivity (low gain) at 250Hz [mV/Pa]

%sensitivity corner frequencies

fc1u=77;            % [Hz]

fc2u=791;           % [Hz]

fc3u=18437;         % [Hz]

fc4u=60;            % [Hz]

% phase corner frequencies

c1u=30;             % [Hz]

c2u=708;            % [Hz]

c3u=19974;          % [Hz]

c4u=60;             % [Hz]
```

```
%% Calculations velocity element sensitivity (High gain/ Low gain)

[su_h]=suh_250Hz./((sqrt(1+(f.^2./fc3u^2))).*(sqrt(1+(fc1u^2./f.^2))).*(sqrt(1+(fc4
u^2./f.^2))).*(sqrt(1+(f.^2./fc2u^2))));

[su_l]=sul_250Hz./((sqrt(1+(f.^2./fc3u^2))).*(sqrt(1+(fc1u^2./f.^2))).*(sqrt(1+(fc4
u^2./f.^2))).*(sqrt(1+(f.^2./fc2u^2))));

%-------------------------------------------------------------------------

%% Calculation of the properties of air and Castor oil

%-------------------------------------------------------------------------

% Thermal conductivity air and Castor oil

k_a=-6.155e-11.*T.^3+6.821e-8.*T.^2+4.743e-5.*T-7.416e-3;

k_c=5.556e-5.*T+0.1637;

%-------------------------------------------------------------------------

% Density at standard atmospheric pressure [kg/m^3]

rho_a=-7.499e-9.*T.^3+1.452e-5.*T.^2-0.01028.*T+3.153;

rho_c=1000./(1.02714+7.04e-4.*TT+9.66e-7.*TT.^2+3.0e-9.*TT.^3-4.91e-4*(p/100)-
2.633e-6*(p/100).*TT-4.04e-9*(p/100).*TT.^2-8.8e-11*(p/100).*TT.^3+1.471e-
6*(p/100)^2+9.2e-9*(p/100)^2.*TT.^2-3.63e-9*(p/100)^3-1.66e-11*(p/100)^3.*TT);

%-------------------------------------------------------------------------

% Specific Heat of air (400 deg C) and Castor oil (40 - 400 deg C)

% Formula for the approximation of the specific heats

cp_a=7.894e-11.*T.^5-1.916e-7.*T.^4+1.820e-4.*T.^3-8.417e-2.*T.^2+19.04.*T-686.8;

cp_c=0.0416.*T.^2-15.336.*T+2684.4;

%% Calculation of partial parameters

D_a=k_a./(rho_a.*cp_a);     % Thermal diffusion coefficient air

D_c=k_c./(rho_c.*cp_c);     % Thermal diffusion coefficient Castor oil

%-------------------------------------------------------------------------

fhc_a=D_a.*rho_a.*cp_a./(2*pi*L*(200e-9*rhoc_SiNi+100e-9*rhoc_pt));        % corner
frequency air [Hz]

fhc_c=D_c.*rho_c.*cp_c./(2*pi*L*(200e-9*rhoc_SiNi+100e-9*rhoc_pt));        % corner
frequency Castor oil[Hz]

%-------------------------------------------------------------------------

fbar_La=(2*pi*L^2./D_a)'*f;         % dimensionless frequency at L (air)

fbar_Lc=(2*pi*L^2./D_c)'*f;         % dimensionless frequency at L (Castor oil)

fbar_Aa=(2*pi*a_a^2./D_a)'*f;       % dimensionless frequency at a (air)

fd_a=D_a./(2*pi.*(a_a^2));          % Second corner frequency (air)

%% Calculation for air with constant distance between the filaments
```

```
% Calculating the factor matrix befor the Bessel function

C_a=(((v_a*a_a.*P)./((1i*pi*ly).*D_a.*k_a))'*exp(1i*2*pi.*f))./fbar_Aa; %

%-------------------------------------------------------------------------

% Numerator of the Bessel function part

numbes_a=1-(sqrt(1i.*fbar_Aa).*besselk(1,sqrt(1i.*fbar_Aa)));

denombes_a=1-((1i./fhc_a')*f).*(besselk(0,sqrt(1i.*fbar_La))-
besselk(0,sqrt(1i.*fbar_Aa)));

%-------------------------------------------------------------------------

% The temperature difference between the filaments

DT_a=C_a.*(numbes_a./denombes_a);       % DT for filaments in air

%% Calculation of Frequency response in air

DT_a_0=(((v_a*a_a.*P)./((2*pi*ly).*D_a.*k_a))).*(log((pi.*a_a)./(2*ly))+0.577); %
DT at f=0 Hz

n=1;

FR_a=zeros(length(DT_a_0),length(f));

for n=1:length(T)

FR_a(n,:)=DT_a_0(n)*((1./sqrt(1+((1./(fhc_a(n).^2'))*(f.^2)))).*(1./sqrt(1+((1./(fd
_a(n).^2'))*(f.^2)))));

n=n+1;

end

%% Calculations for Castor oil at various distances between the filaments

FR_c=zeros(length(DT_a_0),length(f));

n=1;

for n=1:ns

    fbar_Ac=(2*pi.*a_c^2./D_c)'*f;                      % dimensionless frequency
at a (Castor oil)

    fd_c=D_c./(2*pi.*(a_c.^2));                         % Second corner frequency
(air)

    C_c=(((v_c*a_c.*P)./((1i*pi*ly).*D_c.*k_c))'*exp(1i*2*pi.*f))./fbar_Ac;

    numbes_c=1-(sqrt(1i.*fbar_Ac).*besselk(1,sqrt(1i.*fbar_Ac)));

    denombes_c=1-((1i./fhc_c')*f).*(besselk(0,sqrt(1i.*fbar_Lc))-
besselk(0,sqrt(1i.*fbar_Ac)));

    DT_c=C_c.*(numbes_c./denombes_c);                   % DT for filaments in
Castor oil

    DT_c_0=(((v_c*a_c.*P)./((2*pi*ly).*D_c.*k_c))).*(log((pi.*a_c)./(2*ly))+0.577);

    %% Calculate the frequency response in Castor oil

    nn=1;
```

```
    for nn=1:length(DT_c_0)

FR_c(nn,:)=DT_c_0(nn)*((1./sqrt(1+((1./(fhc_c(nn).^2'))*(f.^2)))).*(1./sqrt(1+((1./
(fd_c(nn).^2'))*(f.^2)))));

    nn=n+1;

end

    nn=1;

    % Loop to compare performance at temperatures to performance in air

    for nn=1:length(DT_a_0)

    ratio_DT(nn,:)=DT_a(361,:)./DT_c(nn,:);

    nn=n+1;

    end

    %% Calculation of the ratio of the frequency response

    nn=1;

    % Loop to compare performance at temperatures to performance in air

    for nn=1:length(T) % Loop to compare performance at temperatures to performance
in air

    ratio_FR(nn,:)=FR_a(361,:)./FR_c(nn,:);

    ratio_FR_cold(nn,:)=FR_a(274,:)./FR_c(nn,:);

    nn=nn+1;

    end

    nn=1;

    for nn=1:length(DT_a_0)

    pred1(nn,:)=su_h./abs(ratio_FR(nn,:)); % predicted performance at 313 deg C
using calibration report

    pred11(nn,:)=su_h./abs(ratio_DT(nn,:)); % predicted performance at 313 deg C
using calibration report and raw DT

    nn=nn+1;

    end

    %% Get experimental results

data=xlsread('C:\Users\Marnix\Documents\MATLAB\Thesis\Final
versions\Graphs\Predictions\test_2.xls');

Sv=[data(:,1) data(:,2)];           % get data on velocity sensor only

Sv(:,2)=10.^((Sv(:,2)./20)+9);      % Response in [mV/Pa]

%-------------------------------------------------------------------------

% Plot prediction at different distances between the wires
```

```
figure(100+n)

plot(f,pred1(274,:))            % 313 degrees C

hold on

plot(f,pred1(161,:),'r')        % 200 degrees C

scatter(Sv(:,1),Sv(:,2)./10);

xlabel('Frequency [Hz]','FontSize',14)

ylabel('Sensitivity [mV/Pa]','FontSize',14)

set(findobj('type','axes'),'fontsize',12,'FontWeight','demi')

axis([0 1000 0 0.5])

legend('313 deg C','200 deg C','experiment','313 deg C 100
microns','Location','NorthEast')

tt = strcat({'Predicted sensitivity, no gain, 20% loss for '}, num2str(a_c*1e6),{'
microns'});

title(tt,'FontSize',18,'FontWeight','bold')

figure(200+n)

plot(f,pred11(274,:))       % 313 degrees C

hold on

plot(f,pred11(161,:),'r')   % 200 degrees C

scatter(Sv(:,1),Sv(:,2)./10);

xlabel('Frequency [Hz]','FontSize',14)

ylabel('Sensitivity [mV/Pa]','FontSize',14)

set(findobj('type','axes'),'fontsize',12,'FontWeight','demi')

axis([0 1000 0 5])

legend('313 deg C','200 deg C','experiment','313 deg C 100
microns','fontsize',12,'Location','NorthEast')

tt = strcat({'Predicted sensitivity 140dB using DT, no gain, 20% loss for '},
num2str(a_c*1e6),{' microns'});

title(tt,'FontSize',18,'FontWeight','bold')

%-------------------------------------------------------------------------

figure (1)                % Plot ratio of DT for various distances between the
wires

plot(f,pred1(274,:))

axis([0 1000 0 0.5])

hold all

xlabel('Frequency [Hz]','FontSize',16)

ylabel('Sensitivity [mV/Pa]','FontSize',16)
```

```
legend('20um','40um','60um','80um','100um','fontsize',14,'Location','EastOutside');

title('Predicted sensitivity, no gain at 313 deg
C','FontSize',20,'FontWeight','bold')

figure (2)

plot(f,pred1(161,:))

axis([0 1000 0 0.5])

hold all

xlabel('Frequency [Hz]','FontSize',14)

ylabel('Sensitivity [mV/Pa]','FontSize',14)

legend('20um','40um','60um','80um','100um','Location','EastOutside');

title('Predicted sensitivity, no gain at 200deg
C','FontSize',20,'FontWeight','bold')

figure (3)                % Plot ratio of DT for various distances between the
wires

plot(f,pred11(274,:))

axis([0 1000 0 0.3])

hold all

xlabel('Frequency [Hz]','FontSize',16)

ylabel('Sensitivity [mV/Pa]','FontSize',16)

legend('20um','40um','60um','80um','100um','fontsize',14,'Location','EastOutside');

title('Predicted sensitivity using DT, no gain at 313 deg
C','FontSize',20,'FontWeight','bold')

figure (4)

plot(f,pred11(161,:))

axis([0 1000 0 0.3])

hold all

xlabel('Frequency [Hz]','FontSize',14)

ylabel('Sensitivity [mV/Pa]','FontSize',14)

legend('20um','40um','60um','80um','100um','Location','EastOutside');

title('Predicted sensitivity using DT, no gain at 200deg
C','FontSize',20,'FontWeight','bold')

%-------------------------------------------------------------------------

figure (300+n)

imagesc(f,T(1:274)-273,pred1(1:274,:))

xlabel('Frequency [Hz]','FontSize',14)

ylabel('Temperature [deg C]','FontSize',14)
```

```
colorbar('vert')

caxis([0 .3])

h=colorbar;

ylabel(h,'mV/Pa','FontSize',14)

tt = strcat({'Sensitivity prediction vs filament temperature for '},
num2str(a_c*1e6),{' microns'});

title(tt,'FontSize',18,'FontWeight','bold')

figure (400+n)

imagesc(f,T(1:274)-273,pred11(1:274,:))

xlabel('Frequency [Hz]','FontSize',14)

ylabel('Temperature [deg C]','FontSize',14)

colorbar('vert')

caxis([0 .3])

h=colorbar;

ylabel(h,'mV/Pa','FontSize',14)

tt = strcat({'Sensitivity prediction vs filament temperature using DT for '},
num2str(a_c*1e6),{' microns'});

title(tt,'FontSize',18,'FontWeight','bold')

%-------------------------------------------------------------------------

n=n+1;

a_c=a_c+step;

end

n=1;

for n=1:ns

figure(100+n)

hold on

plot(f,pred1(274,:),'--b')

legend('313 deg C','200 deg C','experiment','313 deg C 100
microns','Location','NorthEast')

n=n+1;

end

for n=1:ns

figure(200+n)

hold on

plot(f,pred11(274,:),'--b')
```

```
legend('313 deg C','200 deg C','experiment','313 deg C 100
microns','Location','NorthEast')

n=n+1;

end

%% predictions at 313 deg Celcius

figure(5)

plot(f,10.*pred1(274,:))

hold on

plot(10.*pred11(274,:),'r')

scatter(Sv(:,1),Sv(:,2));

legend('prediction using approximation','prediction using DT ratio',' averaged
experimental results','Location','NorthEast')

xlabel('Frequency [Hz]','FontSize',16)

ylabel('Sensitivity [mV/Pa]','FontSize',16)

set(findobj('type','axes'),'fontsize',14,'FontWeight','demi')

axis([0 1000 0 1])

title('Sensitivity 140dB, no gain, 20% loss','FontSize',20,'FontWeight','bold')
```

THIS PAGE INTENTIONALLY LEFT BLANK

LIST OF REFERENCES

[1] A. E. Perry, "Introduction," in *Hot-wire Anemometry*, Oxford, Great Britain: Oxford University Press; New York: Clarendon Press; 1982, pp. 1–13.

[2] H. de Bree, "An overview of microflown technologies," *Acta Acust. United Acust.,* vol. 89, pp. 163–172, Jan-Feb, 2003.

[3] C. W. Ng, "Experimental tracking of aerial targets using the Microflown sensor," M.S. thesis, Dept. Phys., Naval Postgraduate School, 2012.

[4] J. V. Caulk "Experimental and theoretical performance of a particle velocity vector sensor in a hybrid acoustic beamformer," M.S. thesis, Dept. Phys., Naval Postgraduate School, 2009.

[5] L. J. Ziomek, "Complex aperture theory," in *Fundamentals of acoustic field theory and space-time signal processing*, Boca Raton: CRC Press, 1995, pp. 405–415.

[6] National Instruments, *National Instruments USB 9234 User Guide and Specifications,* pp. 16–20, 2008.

[7] R. N. Capps, et al., "Transducer fill fluids," in *Handbook of Sonar Transducer Passive Materials*, 1st ed. Washington DC: Naval Research Laboratory, 1981, pp. 159–200.

[8] H. Eckelmann, "Hot-wire and hot-flim measurements in oil," *DISA Info.,* vol. 13, pp. 16–22, 1972.

[9] J.W. van Honschoten, et al., "Analytic model of a two-wire thermal sensor for flow and sound measurements," *J. of Micromech. Microeng.,* vol. 14, pp. 1468–1477, Nov, 2004.

[10] L. E. Kinsler, et al., "Reflection and Transmission," in *Fundamentals of Acoustics,* New York: Wiley, 2000, pp. 149–163.

[11] J. W. van Honschoten, et al., "Optimization of a two-wire thermal sensor for flow and sound measurements," in *the 14th IEEE International Conference on Micro Electro Mechanical Systems,* 2001, pp. 523–526.

THIS PAGE INTENTIONALLY LEFT BLANK

INITIAL DISTRIBUTION LIST

1. Defense Technical Information Center
   Ft. Belvoir, Virginia

2. Dudley Knox Library
   Naval Postgraduate School
   Monterey, California

3. Hans-Elias de Bree
   Microflown Technologies
   Arnhem, Netherlands

4. Prof. dr. ir. F.G.J. Absil
   Royal Netherlands Navy
   Den Helder, Netherlands

5. M.J.M. Hezemans
   Royal Netherlands Navy
   Schagen, Netherlands

6. Jay Adeff
   Naval Postgraduate School
   Monterey, California